Mineralium Deposita (2003) 38: 67–86
DOI 10.1007/s00126-002-0279-2

ARTICLE

Cinzia Maineri · Marco Benvenuti · Pilar Costagliola
Andrea Dini · Pierfranco Lattanzi
Giovanni Ruggieri · Igor M. Villa

Sericitic alteration at the La Crocetta deposit (Elba Island, Italy): interplay between magmatism, tectonics and hydrothermal activity

Received: 6 October 2001 / Accepted: 16 January 2002 / Published online: 2 July 2002
© Springer-Verlag 2002

Abstract The La Crocetta mine near Porto Azzurro (Elba Island, Tuscany, Italy) is an important producer of raw material for the ceramic industry. Exploitation focuses on a pervasively sericitized porphyritic aplite of the Tuscan Magmatic Province, locally known as "eurite", which underwent significant potassium enrichment during sericitic alteration. Eurites are located along the hanging wall of the Elba Centrale Fault, a low-angle extensional lineament of regional significance. A later carbonatization stage, apparently associated with high-angle extensional tectonics, locally overprinted the sericitized facies. It is expressed by carbonate ± pyrite ± quartz veins, with adverse effects on ore quality. Sericitization was accompanied by addition of potassium, and loss of Na (± Ca, Fe). Rubidium was not enriched along with potassium during sericitization, contrary to what would be expected for interaction with late-magmatic fluids. New ^{40}Ar–^{39}Ar data from eurites provide an isochron age of about 6.7 Ma for the sericitization, whereas the age of the unaltered protolith is ca. 8.8 Ma. Field evidence indicates the Elba Centrale Fault to be the main channel for the hydrothermal fluids. On the other hand, the involvement of heat and/or fluids contributed by the Porto Azzurro pluton, which crops out in the La Crocetta area, is ruled out by field, geochemical and geochronological data (^{40}Ar–^{39}Ar age of Porto Azzurro = 5.9 Ma, i.e. significantly younger than the sericitization event). Fluid inclusion studies suggest that sericitization was associated with a low-temperature (< 250 °C) hydrothermal system. Fluids were locally boiling, of variable salinity (4–17 wt% NaCl equiv.), and contained some CO_2 ($XCO_2 \leq 0.027$). Their ultimate source is not unequivocally constrained; meteoric and/or magmatic contributions may be possible. Low-salinity (≤ 2.6 wt% NaCl equiv.), low-temperature (< 250 °C) fluids are associated with the late carbonate veining. They are considered to be of dominantly meteoric nature because of their low salinity. In summary, sericitization at La Crocetta is regarded as the product of a detachment fault-related, low temperature hydrothermal system, resulting from the structurally controlled focusing of meteoric and possibly magmatic fluids. Hence, potential targets for exploration for similar resources are represented by aplitic bodies located in the hanging wall of Elba Centrale Fault.
Electronic supplementary material to this paper can be obtained by using the Springer LINK server located at http://dx.doi.org/10.1007/s00126-002-0279-2.

Keywords Eurite · Feldspathic material · Hydrothermal alteration · Italy · Low-angle tectonics

Editorial handling: H.E. Frimmel

Electronic supplementary material to this paper can be obtained by using the Springer LINK server located at http://dx.doi.org/10.1007/s00126-002-0279-2.

C. Maineri (✉) · M. Benvenuti · P. Costagliola
Dipartimento di Scienze della Terra, Università di Firenze, and CNR-CS Minerogenesi e Geochimica Applicata, Via La Pira, 4, Firenze, Italy
E-mail: cmaineri@geo.unifi.it
Tel.: +39-55-2757507
Fax: +39-55-284571

A. Dini · G. Ruggieri
CNR, Istituto di Geoscienze e Georisorse, Via Moruzzi 1, Loc. San Cataldo, Pisa, Italy

P. Lattanzi
Dipartimento di Scienze della Terra, Università di Cagliari, Via Trentino 51, Cagliari, Italy

I.M. Villa
Mineralogisches und Petrographisches Institut, Universität Bern, Erlachstrasse 9, CH Bern, Switzerland

Introduction

Italy is Europe's largest producer of feldspathic raw materials for ceramic industries, with about 1.8 Mt/year of mined ore (Pearson 1998). A significant part (average 600,000 t/year) of this production comes from southern Tuscany. The two main deposits are La Crocetta (Elba Island) and Botro ai Marmi (near Campiglia Marittima)

source: https://doi.org/10.7892/boris.87732 | downloaded: 12.10.2024

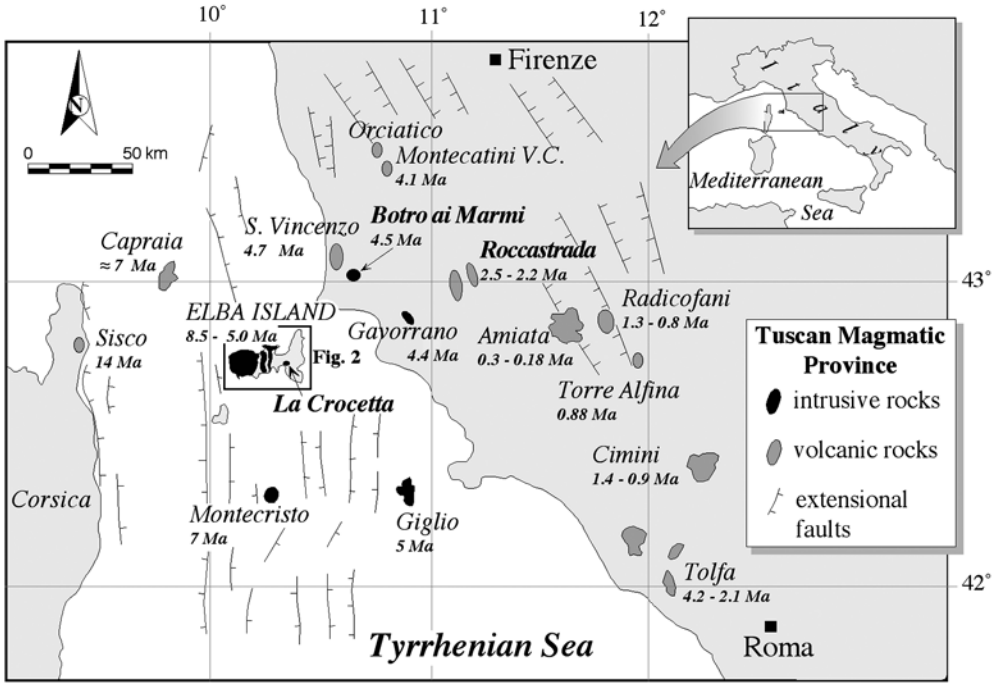

Fig. 1 Location of Elba Island in the northern Tyrrhenian Sea. Also shown are the main outcrops of igneous rocks belonging to Tuscan Magmatic Province, and their age in Ma (*numbers* next the outcrops)

(Fig. 1). In both localities, the quarried rocks are altered magmatic rocks of the Miocene–Pleistocene Tuscan Magmatic Province (TMP; Marinelli 1955, 1959; Serri et al. 1991; Innocenti et al. 1992, and references therein). Their peculiar potassium-rich (7 to 11 wt% K_2O) and Fe–Ca–S-poor compositions make them of high commercial quality. It is, therefore, of interest to study the hydrothermal processes that have produced these unique alteration features. This paper focuses on the La Crocetta deposit, with the ultimate goal of developing a descriptive and genetic model, which may be useful in the exploration for similar products in other hydrothermal systems.

Regional geology

Elba Island is located in the northern Tyrrhenian Sea, 10 km offshore of the Tuscan coast (Fig. 1). The island belongs to the Northern Apennines mountain chain, built up during the large-scale, Late Tertiary collision between the European and African (Adria promontory) plates. The geology of Elba Island (Fig. 2) comprises several thrust complexes, which were emplaced during this Alpine–Apennine orogeny, and post-orogenic magmatic rocks of the TMP (Trevisan 1950; Marinelli 1955, 1959; Barberi et al. 1967, 1969a, 1969b; Bortolotti et al. 2001).

Trevisan (1950) recognized five (I–V) major thrust complexes, which were assigned to either Tuscan palaeodomain (complexes I, II, and III) or to Ligurian oceanic realm (complexes IV and V). The latter two are particularly relevant for this paper because the La Crocetta deposit is embedded in complex V, close to the contact with the underlying complex IV. Complex V, the uppermost structural unit, essentially consists of two members. The lower one, a Palaeocene–Eocene pelitic (argillites, calcarenites and sandy marls) succession, is interbedded with ophiolitic breccias, is strongly tectonized and has an eastward sense of movement (Keller and Pialli 1990). The upper member consists of Cretaceous flysch, basically made up of 0.5- to 1.5-m-thick limestones beds, calcareous shales and feldspathic sandstones.

Complex IV, on western Elba Island, consists of Jurassic ophiolitic rocks and overlying Late Jurassic–Middle Cretaceous chert, limestone and argillite. They show metamorphic aureoles related to emplacement of a magmatic body belonging to the TMP, namely the Monte Capanne pluton, which outcrops 10 km to the west. Rubidium–Sr and U–Pb dates for emplacement of the Monte Capanne pluton are scattered between 7.0 and 5.8 Ma (Juteau et al. 1984; Ferrara and Tonarini 1985; Dini 1997). However, late-plutonic mafic dikes (OGP, see below) show a ^{40}Ar–^{39}Ar isochron age of 6.85 ± 0.03 Ma (Dini and Laurenzi 1999). This suggests that the most likely emplacement age for the Monte Capanne pluton is close to 7.0 Ma.

Other post-orogenic magmatic rocks belonging to TMP include the monzogranitic Porto Azzurro pluton, a laccolith complex of subvolcanic porphyritic rocks (PR; Westerman et al. 2000) and the Orano granodioritic porphyries (OGP). The latter comprise the above mentioned mafic dike swarms that cut the Monte Capanne pluton, and also cut rocks of the laccolith complex (Fig. 2). Rubidium–Sr and K–Ar emplacement ages for the Porto Azzurro pluton are between 6.2 and 5.0 Ma, as recalculated from the original data of Saupè et al. (1982) using Isoplot software (Ludwig 2001).

On west-central Elba Island, several units can be distinguished in the porphyritic laccolith complex. These include the Capo Bianco porphyritic aplite unit (Rb–Sr age ≈8 Ma; Dini 1997; Dini et al. 2002), and three different monzogranitic porphyries (Rb–Sr and ^{40}Ar–^{39}Ar ages of 8.0–7.2 Ma; Dini and Laurenzi 1999; Dini et al. 2002). According to recent geological reconstructions (Dini 1997; Westerman et al. 2000), the Capo Bianco porphyritic aplites were emplaced as two sills at different structural levels: the lower one, exposed on western Elba Island (Marciana area), occurs within rocks of complex IV, very close to the contact with rocks of the overlying complex V. The upper body intruded the lower to middle parts of complex V, and presently outcrops near Portoferraio and at the La Crocetta mine (Figs. 2 and 3d). Specifically, the outcrop at La Crocetta is interpreted as the bottom part of the upper Capo Bianco porphyritic aplite sill.

Top-to-the-east extension along the Elba Centrale detachment fault, (CEF), which occurs at the bottom of complex V (Fig. 3b) on the west-central part of the island, is strongly linked to the emplacement of the subvolcanic porphyritic units and the Monte Capanne pluton (Bouillin et al. 1994; Daniel and Jolivet 1995;

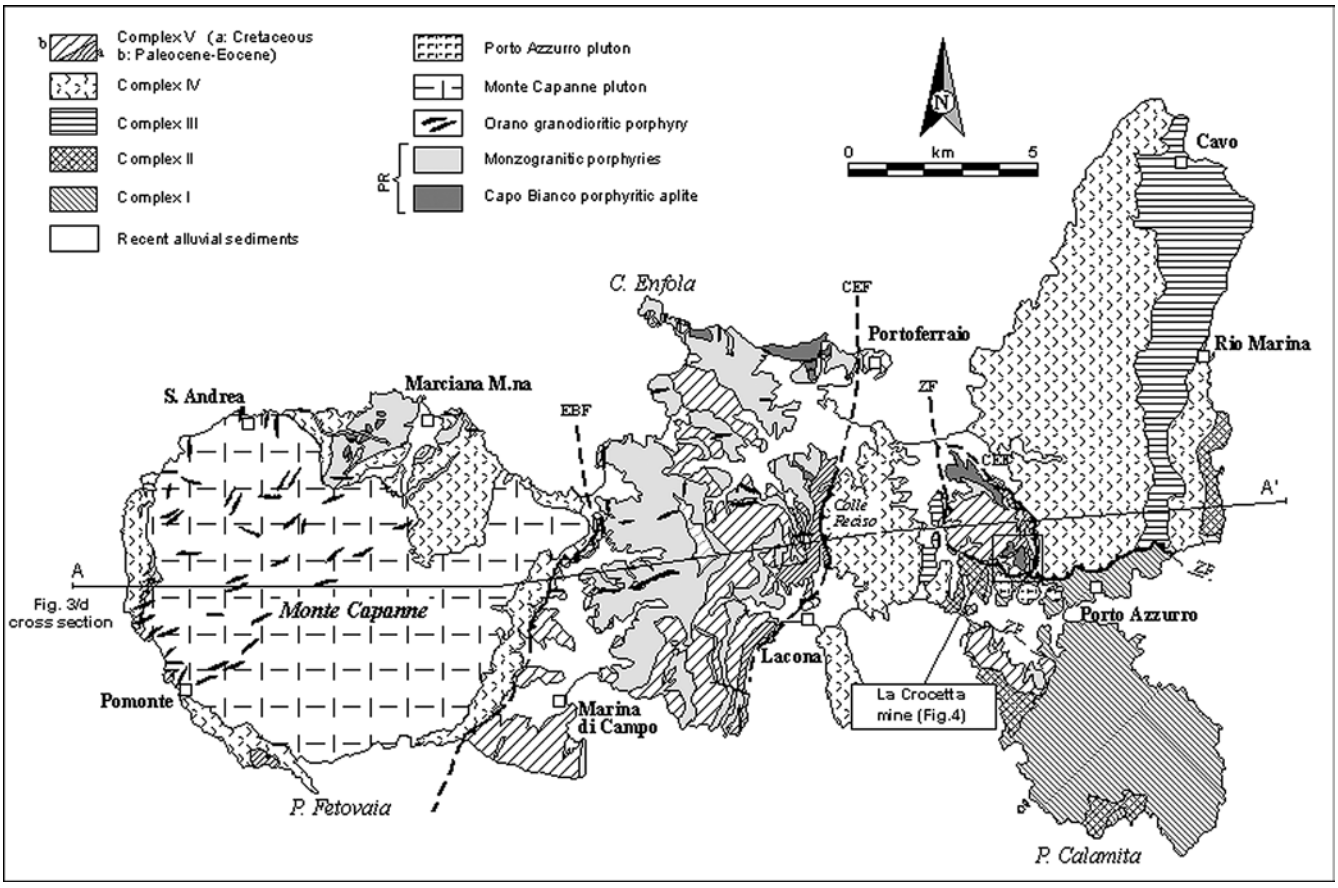

Fig. 2 Geology of Elba Island (modified after Dini et al. 2002). *EBF* Eastern Border fault; *CEF* Elba Centrale detachment fault; *ZF* Zuccale fault

Westerman et al. 2000). This fault controlled the approximately 10 km of eastward translation of rocks of complex V, along with the embedded magmatic rocks (see Fig. 3a, b), from their original position on the top of the Monte Capanne pluton (Trevisan 1950). Minor low-angle normal faulting on the Elba Centrale fault surface may have started during emplacement of the laccolith complex and formation of the dome underlain by the Mt. Capanne pluton. However, the 10 km of eastward displacement occurred after both the development of the Mt Capanne thermal aureole and the emplacement of the 6.85-Ma OGP dike swarm (Fig. 3b–d). The Capo Bianco porphyritic aplite horizon in the Marciana area, located below the detachment surface, basically remained in its original position.

At several localities (Lacona, Colle Reciso and Portoferraio) where the Elba Centrale fault intersects the topographic surface, blocks of porphyries that are deformed by fault movement are hydrothermally altered. They contain abundant hydrothermal quartz and muscovite, with grains exhibiting clear syn-deformational features, such as crystal growth parallel to strain directions (Marinelli 1955; Dini, unpublished data). This suggests that fluid flow was coeval with motion along the detachment surface.

At 6.2–5.0 Ma, the emplacement of Porto Azzurro pluton beneath the Elba Centrale fault (cf. Fig. 3b–d) caused a local topographic and structural high, which both hindered movement along the fault surface to the west of the intrusion and initiated a new easterly-directed tectonic slip. The latter mainly took place along another major low-angle fault, the Zuccale fault (ZF), localizing complex V in its present position (Fig. 3c, d), 15 km east of Monte Capanne (Pertusati et al. 1993; Dini and Tonarini 1997). The last tectonism on Elba Island is mainly represented by N–S-trending high-angle extensional faulting (Fig. 3c, d), which affected the entire northern Tyrrhenian basin. This tectonism ended before 3.5 Ma (Zitellini et al. 1986; Keller and Pialli 1990).

Geology of La Crocetta mine

The La Crocetta mine is located in the eastern part of Elba island, about 2.5 km north-west of the town of Porto Azzurro (Fig. 2). The local geology is characterized by the Capo Bianco porphyritic aplites and subordinated monzogranitic porphyries, which are emplaced as large sills and dikes that vary in thickness from about 10 to 100 m. The intrusions occur within the lowermost part of complex V, at the contact between Cretaceous flysch and Palaeocene–Eocene pelite (Fig. 3). The general orientation of the sills follows the flysch bedding (strike 170–180°N and dip 40–50°W). In particular, the main stopes in the mine exploit a large, hydrothermally-altered Capo Bianco porphyritic aplite body that was intruded along the contact, and cut by a small dike of monzogranitic porphyry (Fig. 4).

In the mine area, the juxtaposition of the porphyritic rocks over the Porto Azzurro pluton is clearly tectonic, and related to movements of the Zuccale fault, which cuts the plane of the older Elba Centrale fault (Fig. 3b–d). In porphyritic bodies and rocks of complex V above the Zuccale fault surface, contact metamorphism is weak to absent. In contrast, rocks of complex I that were intruded

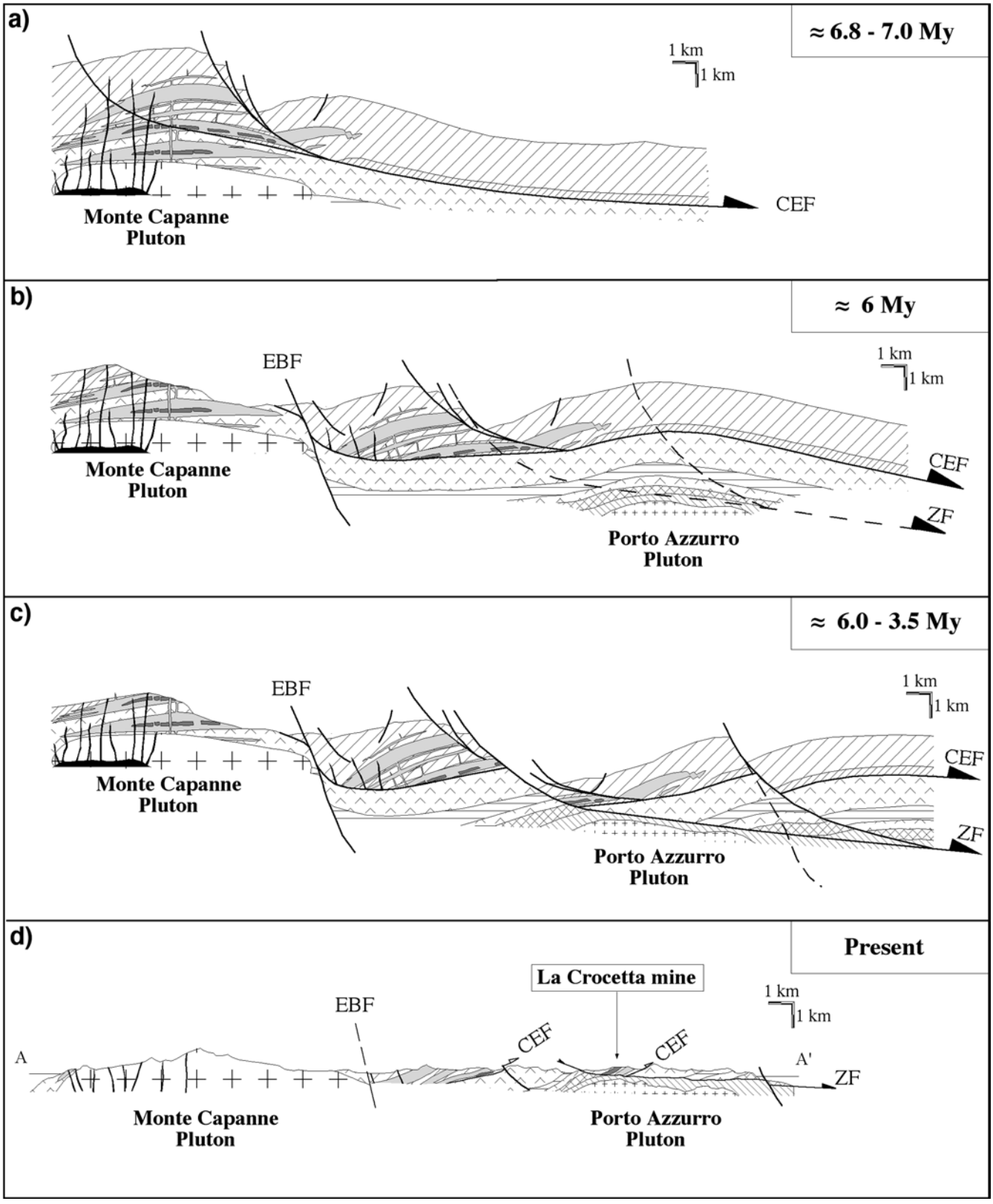

by the Porto Azzurro pluton in the fault footwall show a strong thermal overprint (Pertusati et al. 1993). This is a convincing evidence that the original Porto Azzurro contact aureole was displaced by the Zuccale fault, according to the models of Trevisan (1950) and Marinelli (1959).

The material mined at La Crocetta, the so-called 'eurite', is a porcelaneous whitish rock with high K_2O

◀

Fig. 3a–d Tectono-magmatic evolution of Elba Island. **a** Schematic E–W cross section of Elba Island: geological reconstruction of primary setting of the porphyritic rocks and emplacement within thrust units (after Dini 1997). **b** Eastward translation of porphyritic rocks units caused by movement on the Elba Centrale fault (CEF) and emplacement of the Porto Azzurro pluton (see text for details). **c** Onset of motion along the Zuccale fault (ZF), which was responsible for the ultimate position of the porphyritic rocks units above the Porto Azzurro pluton, along with final N–S vertical extension. **d** Present geological section of Elba Island along A–A′ in Fig. 2. See Fig. 2 for legend

and low Na_2O ($K_2O/Na_2O \cong 60$), arising from a pervasive hydrothermal alteration of the Capo Bianco porphyritic aplite. This pervasive alteration is typical of only the La Crocetta area; all other extensive outcrops of Capo Bianco porphyritic aplite in the Portoferraio and Marciana areas are weakly altered or may locally display a late magmatic tourmalinization (see below); unaltered rocks typically display a K_2O/Na_2O ratio of about 1. The Capo Bianco aplite is also mined (at Marciana) as a raw material for ceramics.

In the south-western part of the mine, a peculiar, carbonate-rich facies, known as "candor", is associated with the development of carbonate ± quartz-pyrite veins up to decimetric width, which overprint the pervasive, potassium-rich alteration. These veins strike mainly N–S, have variable dips, and may either be entirely hosted by porphyritic rocks or extend into the surrounding flysch. The timing of formation of this vein system is not clear. It could be related to the regional late-stage, high-angle extensional tectonics or, perhaps more likely, to the development of conjugate faults related to movements along the Elba Centrale fault. The "candor" facies is of lower economic value.

Methods and instruments

Whole-rock chemical analyses were done at Dipartimento di Scienze della Terra, Università di Firenze, Italy, and Dipartimento di Scienze della Terra, Università di Pisa, Italy. Major and trace elements were determined by X-ray fluorescence, except for Fe^{2+} (by titration against $KMnO_4$) and Mg, Na and K (by AAS). Loss on ignition (LOI) was measured by gravimetry at 1,000 °C.

To perform mass balance calculations of unaltered vs altered rocks, the physical properties of samples [weight (W), real (Vr) and bulk volume (Vb), density (γ) bulk density (γs), total open porosity (P)] were determined at Centro di Studio sulle Cause di Deperimento e sui Metodi di Conservazione delle Opere d'Arte, CNR, in Firenze. The 1.5×1.5×3-cm samples were first dried at 60 °C, and their weight was determined. Then, both the real volume Vr (using a Quantachrome Helium picnometer) and the bulk volume Vb (using a Chandler Engineering Mercury picnometer) were measured. The density was calculated as $\gamma = W/Vr$, bulk density as $\gamma s = W/Vb$, and total open porosity as $P = 100(Vb–Vr/Vb)$.

Microthermometry and Raman analyses of fluid inclusions were carried out on 100-μm-thick, doubly polished wafers at Dipartimento di Scienze della Terra, Firenze, and at Istituto Internazionale per le Ricerche Geotermiche of CNR in Pisa, by using the Chaimexca and Linkam THMSG 600 heating–freezing stages. Both stages were calibrated with pure H_2O synthetic fluid inclusions, and natural pure CO_2 inclusions. Accuracy was estimated in the order of ±0.2 °C during freezing below 10 °C, and ±2.0 °C when heating in the temperature range of 50–350 °C. Raman analyses were performed at Centro di Studio Minerogenesi e Geochimica Applicata of CNR in Firenze, by using a Jobin-Yvon S 3000 spectrometer, equipped with a Spectraphysics Ar^+ laser source (514.5 and 488 nm), a BH 2 Olympus microscope, and a CCD-type, liquid-nitrogen cooled detector.

The molar fraction of CO_2 (XCO_2) and the salinity expressed in wt% NaCl equiv. of CO_2-bearing liquid-rich inclusions (i.e. L1 type inclusions, see below) were estimated using the computer program ICE of Bakker (1997) on the basis of clathrate melting temperature (T_{mcl}), final ice melting temperature (T_{mi}), composition of the gas phase, and volume fraction of the gas phase. Trapping pressures for some of these inclusions, assumed to have been trapped during boiling, were computed directly from their microthermometric data and composition, by using the method of Barton and Chou (1993).

The maximum XCO_2 of liquid-rich, CO_2-poor inclusions (i.e. L2 and L3 type inclusions, see below) was also calculated by the program ICE of Bakker (1997). The salinity of these inclusions was calculated from T_{mi} values, using the equation of Bodnar and Vityk (1994). The maximum trapping pressure of L2 inclusions, presumably formed during the boiling process, were calculated using the method of Barton and Chou (1993), whereas pressure corrections for L2 and L3 inclusions that were not trapped under boiling conditions were modelled using Zhang and Frantz's (1987) equation of state.

Two different compositions (in terms of XCO_2 and XH_2O) of a vapour-rich inclusion (i.e. V type inclusion, see below) were estimated using the computer program Q2 of Bakker (1997). This was done on the basis of T_{mcl}, CO_2 homogenization temperature (T_{hCO2}), composition of the gas phase and two distinct volume fractions of the gas phase.

Mineral separates for radiometric analyses were obtained by conventional heavy liquid and magnetic separation. Grain sizes of selected samples were comprised between 100 and 150 μm. Dating by Ar–Ar was performed at Mineralogisches Petrographisches Institut, Universität Bern, Switzerland, using the analytical procedure described in detail by Villa et al. (2000).

The alteration processes at La Crocetta

Mineralogy and textures

Unaltered Capo Bianco porphyritic aplite bodies are mainly composed of 1–5-mm-diameter microphenocrysts of oligoclase–albite, quartz, K-feldspar (Or_{78}–Or_{88}), and muscovite. These are hosted in a very fine groundmass having a grain size of between 5 and 50 μm, composed of euhedral crystals of albite embedded in an equigranular aggregate of xenomorphic quartz, K-feldspar, albite and muscovite. Accessory minerals include euhedral xenotime, monazite, zircon, apatite and rare Nb–Ta oxides. Rocks of the Capo Bianco porphyritic aplite are classified as subalkaline, peraluminous, alkali-feldspar granites (Dini 1997). They are strongly enriched in some lithophile elements, such as B, Be, Li, Rb, Cs, Ta, Nb, Y, Sn and W, whereas they show very low contents of Sr, Ba, Th and Zr. The Capo Bianco porphyritic aplites have a flat REE pattern, with a very strong negative Eu anomaly (Dini 1997).

The monzogranite porphyries are subalkaline, and slightly less peraluminous than the Capo Bianco porphyritic aplites. The Orano granodioritic porphyries dikes, the most mafic of the magmatic bodies, are metaluminous, and show low rubidium contents and strong enrichment in some compatible (Mg, Fe, Cr and Ni) and incompatible (LREE, Ba and Sr) elements. A

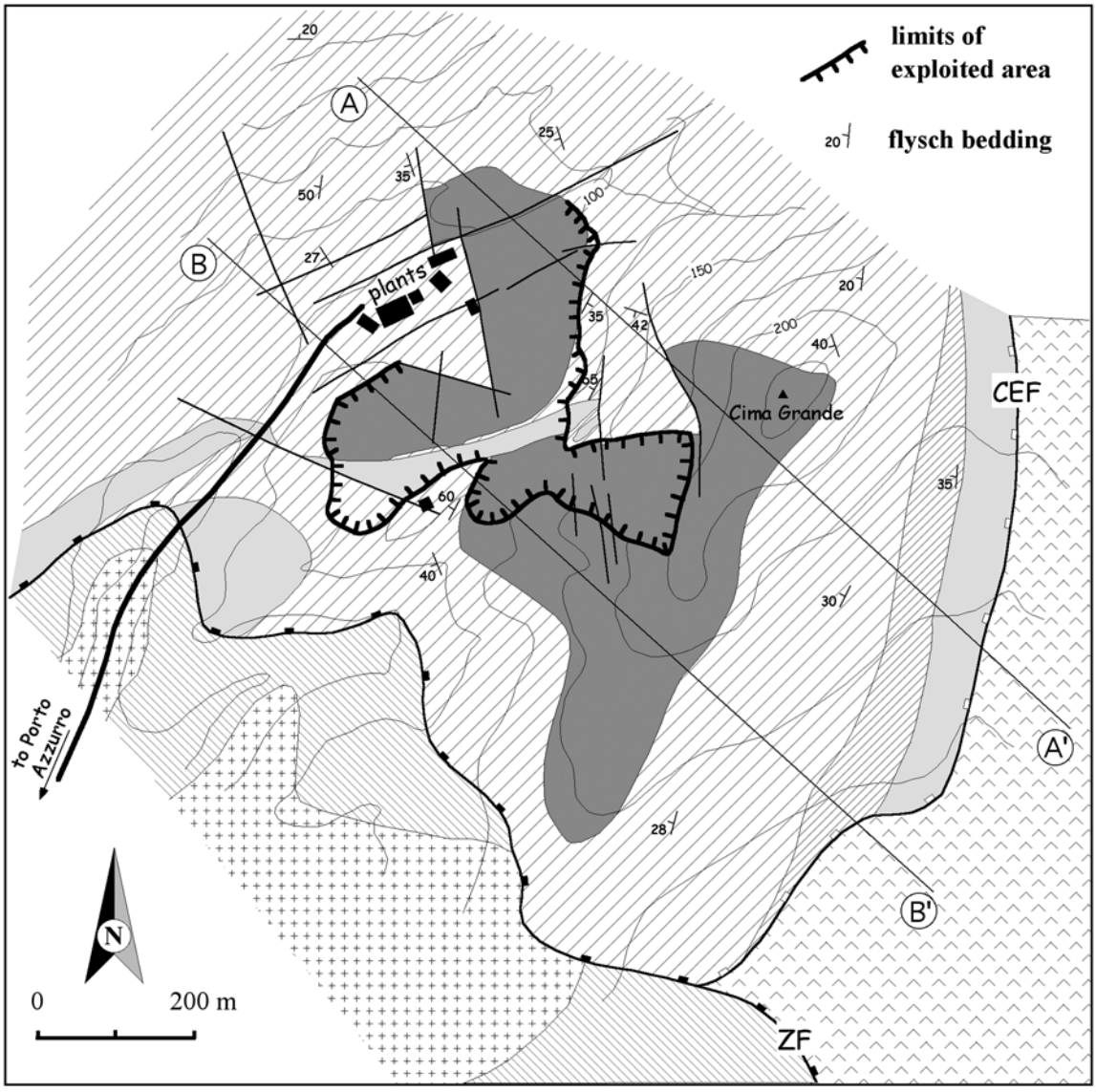
limits of exploited area
flysch bedding
plants
Cima Grande
CEF
ZF
to Porto Azzurro
A
A'
B
B'
N
0
200 m

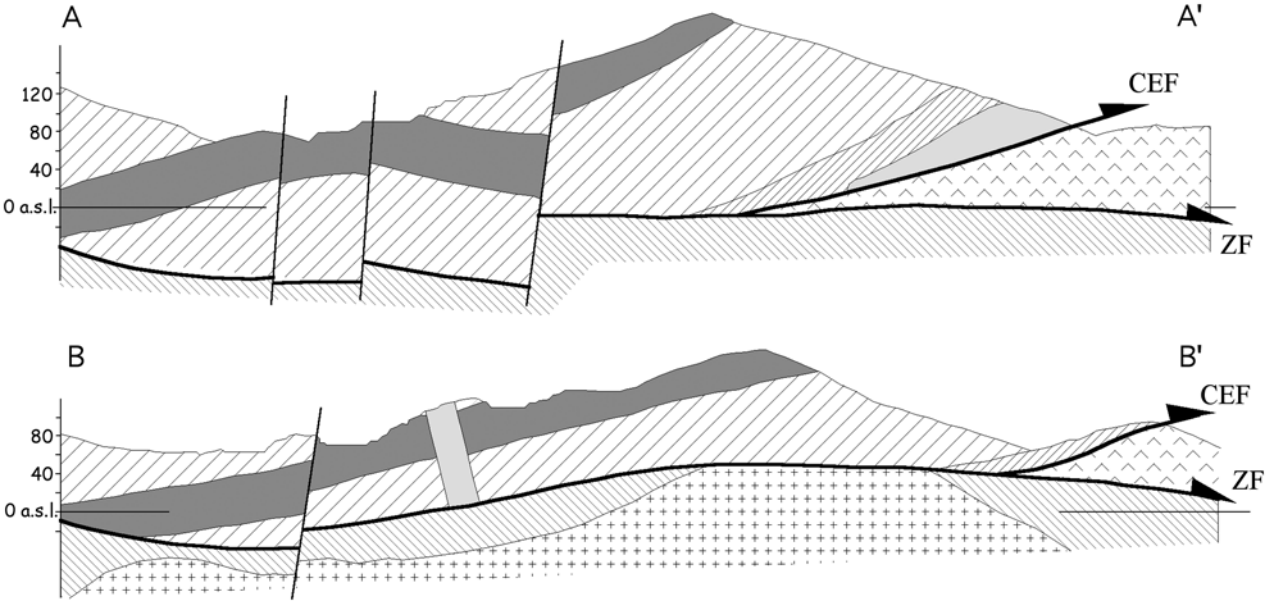
A
A'
CEF
ZF
120
80
40
0 a.s.l.
B
B'
CEF
ZF
80
40
0 a.s.l.

◀

Fig. 4 *Top* Geological map of the La Crocetta mine (*CEF* Elba Centrale detachment fault; *ZF* Zuccale fault). *Bottom* Geological cross sections of the mining area along *A–A′* and *B–B′*. See Fig. 2 for legend

summary of geochemical data for all magmatic lithotypes outcropping in both the La Crocetta and Marciana areas is presented in Table 1.

Late- to post-magmatic alteration of the Capo Bianco porphyritic aplites includes three main stages that never occur together. The first stage, considered to be late magmatic by Dini (1997), is characterized by the occurrence of tourmaline (schorl) and muscovite in spheroidal aggregates, both replacing feldspars. The aggregates are of variable size and frequency, and affect only minor rock volumes. Such aggregates show a general tendency of increasing size with higher levels in the upper Capo Bianco porphyritic aplite (e.g. Portoferraio outcrops), where they may reach 10 cm in diameter. Rocks affected by this alteration event do not occur at the La Crocetta mine. The relatively high iron content, caused by the abundant tourmaline, makes them not suitable for raw ceramic material.

In contrast, the subsequent (second) alteration stage produced rocks of economic importance. It was characterized by the extensive replacement of albitic plagioclase and feldspars with fine-grained sericite, clearly distinguishable from the earlier large muscovite flakes of the spheroidal aggregates. Sericitization was accompanied by the precipitation of fine-grained (< 5 μm) quartz intergrown with sericite or, less frequently, forming thin veinlets or micro-vugs. Sericite often fully replaces plagioclase whereas replacement of K-feldspar may be restricted to crystal rims. Sericitization, in general, increases eastward and downward through the Capo Bianco porphyritic aplite (i.e. towards the CEF surface, Fig. 3); it is particularly extensive only at La Crocetta. The main material exploited at La Crocetta, eurite, is actually the strongly sericitized Capo Bianco porphyritic aplite, where all feldspars have been almost completely replaced. Consequently, La Crocetta is, in fact, best defined as a hydrothermal sericite deposit, where the sericite is recovered for ceramics.

The final (third) alteration stage is almost exclusive of La Crocetta. It is expressed by microscopic to macroscopic veins (thickness from some hundred of microns up

Table 1 Mean chemical composition and physical properties for representative rock types. γ = Density; γs = bulk density (see the 'Methods and instruments' paragraph for their definition); *n.m.* = not measured; *n.d.* = not detected

Rock type	Monzogranitic Porphyry		Orano granodioritic Porphyry (OGP)		Capo Bianco Porph. aplite		Eurite		Candor	
No. of samples	12		6		4		9		6	
Data source	This work		Dini (1997)		This work		This work		This work	
	Mean	SD	Mean	SD	Mean	SD	Mean	SD	Mean	SD
Major elements (wt%)										
SiO_2	68.98	1.55	64.09	1.10	73.52	0.45	70.63	3.43	68.01	5.16
TiO_2	0.33	0.06	0.64	0.04	0.00	0.00	0.00	0.00	0.14	0.16
Al_2O_3	16.42	1.08	15.67	0.38	15.73	0.29	17.39	1.84	16.51	1.62
Fe_2O_3	0.52	0.42	1.10	0.27	0.24	0.26	0.24	0.15	0.61	0.36
FeO	1.40	0.46	2.94	0.20	0.37	0.04	0.26	0.09	0.36	0.36
MnO	0.03	0.01	0.07	0.01	0.07	0.02	0.03	0.02	0.05	0.04
MgO	0.78	0.28	3.24	0.75	0.29	0.30	0.28	0.06	0.53	0.33
CaO	1.63	0.56	3.57	0.75	0.43	0.25	0.64	1.22	3.18	3.04
Na_2O	3.19	0.77	3.21	0.30	4.00	0.08	0.13	0.06	0.09	0.03
K_2O	4.39	0.48	3.75	0.25	4.10	0.42	7.92	1.55	6.48	0.51
P_2O_5	0.11	0.03	0.21	0.04	0.04	0.00	0.01	0.01	0.05	0.04
LOI	2.22	0.84	1.51	0.38	1.24	0.26	2.26	0.69	3.98	1.39
Tot	100.00		100.00		100.03		99.79		99.99	
Trace elements (ppm)										
Rb	321	26	204	22	596	63	633	104	465	79
Sr	188	71	378	122	33	7	23	16	109	102
Y	22	6	19	1	34	3	40	5	29	9
Zr	123	13	173	23	32	1	43	3	73	38
Nb	13	2	12	1	20	4	20	2	16	2
Ba	332	119	433	48	37	7	225	57	353	173
La	26	4	66	32	3	1	9	3	14	7
Ce	51	8	102	20	7	1	44	20	71	28
V	25	5	66	14	n.d.	n.d.	n.d.	n.d.	n.d.	n.d.
Cr	19	6	95	25	n.d.	n.d.	n.d.	n.d.	n.d.	n.d.
Co	4	2	13	2	n.d.	n.d.	n.d.	n.d.	n.d.	n.d.
Ni	8	3	47	28	n.d.	n.d.	n.d.	n.d.	n.d.	n.d.
Physical properties										
γ (g/cm^3)	n.m.	n.m.	n.m.	n.m.	2.63	0.02	2.66	0.01	2.67	0.01
γs (g/cm^3)	n.m.	n.m.	n.m.	n.m.	2.56	0.01	2.31	0.03	2.46	0.02
Porosity (%)	n.m.	n.m.	n.m.	n.m.	2.50	0.49	13.48	1.27	7.77	0.76

to some decimetres) filled by carbonate minerals (mainly calcite), with subordinate quartz and pyrite. At the microscale, one can observe the calcite ± quartz ± pyrite micro-veins cutting the sericitic alteration assemblage; locally, the magmatic quartz phenocrysts of the Capo Bianco aplites may also be cut by the third stage microveins. More rarely, third stage quartz occurs as small overgrowths on magmatic quartz phenocrysts. Where the microveins are particularly abundant, the resulting rock (of lower economic value) is the candor facies.

The monzogranite porphyries at La Crocetta also show variable degrees of sericitization. Outside the mining area, the monzogranite and the Orano granodioritic porphyries exhibit widespread alteration of primary biotite and plagioclase to chlorite and sericite ± calcite, respectively. The Porto Azzurro pluton shows weak hydrothermal alteration, reflected by the occurrence of a stockwork of chlorite–epidote–albite–calcite veinlets, which extends into the rocks of the contact aureole. The more distal Monte Capanne pluton was generally not affected by these alteration processes.

Mass balance calculations

To establish the nature and extent of the main alteration processes responsible for the development of the eurite facies at La Crocetta, we compared the major, minor and trace element composition of these altered rocks with those of their 'fresh' counterparts (i.e. the Capo Bianco porphyritic aplites), by means of mass balance calculations. Element gains and losses were calculated by the mass balance isochon method of Grant (1986), on the basis of data reported in Table 1. In a C_1 (Eurite) vs C_0 (Capo Bianco porphyritic aplite) diagram (Fig. 5a), the position of SiO_2 and Al_2O_3 with respect to the isochon reflects substantial concentration constancy, i.e. they behaved as immobile components. Eurites show a strong enrichment in bulk K_2O and LOI, whereas Na_2O, CaO and Sr were apparently leached during sericitization. The loss of Na_2O (and possibly CaO) is in agreement with the textural observation of plagioclase replacement by sericite. On the other hand, CaO, Sr and Fe_2O_3 were gained by sericitized rocks affected by the third-stage carbonatization event (Fig. 5b). Contrary to what we would expect, rubidium is not co-enriched with potassium in the eurites. As a consequence, the K/Rb weight ratio in eurites is much higher (about 110–130) than in the unaltered Capo Bianco protolith (about 60). The enrichment of barium in most altered samples, and its positive correlation with K_2O, LOI and CaO, together with the absence of primary barium-rich mineral phases, suggest that this element, other than in relics of primary feldspar, may be present in white mica and late-stage carbonate minerals. Other trace elements (Zr, Y and Nb) appear to have been only slightly mobile in the alteration processes. A significant rock volume decrease accompanying alteration of the Capo Bianco porphyritic aplite protolith is clear from the C_1/C_0 diagrams.

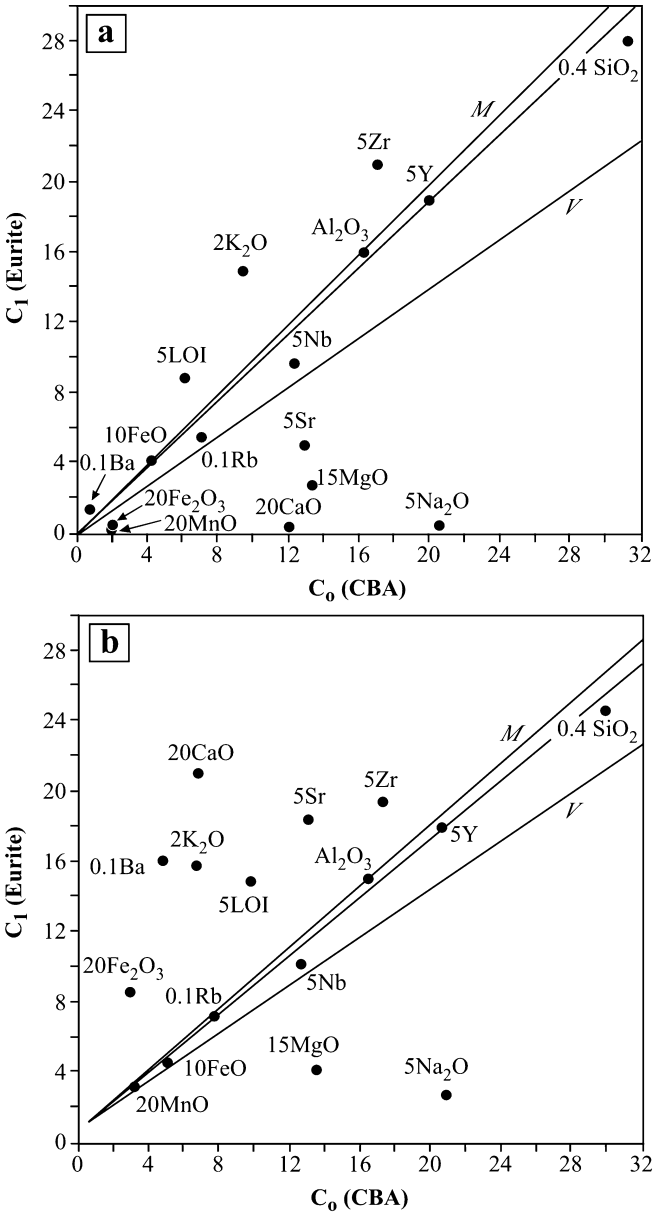

Fig. 5 Isochon diagrams showing chemical changes that occur during Capo Bianco porphyritic aplite sericitization (**a**) and subsequent carbonate alteration (**b**). C_0 and C_1 refer to unaltered (Capo Bianco porphyritic aplite) and altered (eurite) rocks, respectively. *M* and *V* indicate constant mass and constant volume conditions, respectively

^{40}Ar–^{39}Ar geochronology

Dating using ^{40}Ar–^{39}Ar analyses was carried out to establish the chronological relationships between magmatic and hydrothermal events in the mining area. As shown in Table 2, three samples were analysed: (1) a late magmatic muscovite from the slightly altered Capo Bianco porphyritic aplite protolith in the Portoferraio area (ORB I); (2) a sericite-rich eurite sample from the mine area (G7); and (3) biotite from the Porto Azzurro pluton (AZ). Detailed information on ^{40}Ar–^{39}Ar analytical results is reported in the electronic supplementary Table.

Table 2 Description and age of samples selected for ^{40}Ar–^{39}Ar dating. In parentheses, contaminant phases. *chl* Chlorite; *pg* plagioclase; *qz* quartz

Sample	Rock type and locality	Mineral separate	Purity	Weight (mg)	Grain size	Isochron age (Ma)
AZ	Monzogranite (Porto Azzurro)	Biotite	98% (chl)	24.4	> 160 μm	5.9 ± 0.2
ORB I	Unaltered CBA (Portoferraio)	Muscovite	> 99%	34.12	> 150 μm	8.9 ± 0.2
G7	Eurite (Crocetta)	Sericite	ca. 90% (qz, pg)	14.94	112 μm/4 μm	6.7 ± 0.1

The age spectra shown in Fig. 6a indicate significantly different ages for the three samples: about 8.5 Ma for ORB I muscovite, about 7 Ma for G7 sericite and about 6 Ma for AZ biotite. For comparison, the age spectrum of Orano Granodioritic Porphyry (Dini and Laurenzi 1999) is shown in Fig. 6b. Second-order complexities (i.e. deviation by ca. 0.2 Ma), shown by all spectra, deserve further discussion. The ^{40}Ar–^{39}Ar method offers the possibility of recognizing the presence of small amounts of minerals other than mica in the samples, in particular calcium-bearing minerals (see the review by Villa 2001). Therefore, the steps with lowest Ca/K ratios (calculated from the $^{37}Ar/^{39}Ar$ ratio) reflect degassing of micas least contaminated by impurities. Moreover, multiple mica generations can be recognized during sample degassing by their Cl/K ratios (chlorine contents being known by the total production of ^{38}Ar), reflecting variable OH–Cl substitution (Villa et al. 1997, 2001). Specifically, by plotting the Cl/K ratio vs. age, one can combine the identification of successive mica generations with an estimate of their age.

The diagram shown in Fig. 6c for the AZ biotite reports only the five steps having a Ca/K ratio < 0.1, omitting steps with higher Ca/K ratios, which are ascribed to calcium-rich impurities. The diagram reveals a very limited range in the Cl/K ratio (0.0147–0.0152), and no clear correlation with age. The average of the five steps gives an age of 5.9 ± 0.2 Ma. This age is ten times less precise than the error on individual steps because steps scatter more than the purely analytical error. Hence, 5.9 ± 0.2 Ma can be taken as the best estimate of the age of the AZ biotite, with a conservative error assignment. This value is identical to our re-evaluation of the Saupè et al. (1982) Rb–Sr data, where an isochron age of 5.8 ± 0.2 Ma (initial $^{87}Sr/^{86}Sr = 0.7145$) has been recalculated using data from four biotites and the whole rock with the lowest strontium isotopic composition.

Muscovite (ORB I) and sericite (G7) have much lower Cl/K ratios with respect to AZ biotite, but, more importantly, the relative variations are much higher (Fig. 6d). Interestingly, in the Cl/K vs. age plot, ORB I and G7 define a colinear trend that can be described by the curve shown in Fig. 6d. The data relationship suggests that in both eurite and in its protolith, respectively, neither a purely hydrothermal nor a purely magmatic mica can be found. Both mica generations are intimately mixed in different proportions, depending on the rock in which they occur. The magmatic mica retains the highest Cl/K ratio and the oldest age, whereas the opposite holds for the hydrothermal mica generation. The spreading of the data in Fig. 6d poses some problems for exact mica age estimates. However, a reasonable approximation can be obtained by considering the age corresponding to data with the highest and lowest Cl/K ratio. By taking a Cl/K ratio of about zero as representative of the purest hydrothermal mica, the intercept of the correlation curve of Fig. 6d with the *y* axis (Cl/K = 0), corresponds to an age of 6.7 ± 0.1 Ma. We suggest that this represents the most likely age of sericitization. The age of unaltered magmatic muscovite can be less precisely defined; however, from Fig. 6d, we estimate that the pure magmatic muscovite end member may have $Cl/K = 0.0038 \pm 2$ and, therefore, an age of 8.8 ± 0.2 Ma. This value is older than previously reported Rb–Sr ages for the Capo Bianco porphyritic aplite in the Portoferraio area (7.95 ± 0.1; Dini 1997). A possible explanation for this 1-Ma discrepancy is that the Capo Bianco porphyritic aplite did not behave as a closed system, and was (partially) affected by post-emplacement hydrothermal activity. Therefore, the apparent younger age obtained by Dini (1997) may reflect both a partial hydrothermal recrystallization of magmatic muscovite phenocrysts and a perturbation of the Rb–Sr whole-rock system. In any case, the most important conclusion is that the best age estimate for sericitization is definitely younger than the crystallization of the Capo Bianco porphyritic aplite, and definitely older than emplacement of the Porto Azzurro pluton. Hence, sericitization cannot be linked to magmatic fluids related to either the Capo Bianco porphyritic aplites or the Porto Azzurro pluton.

Fluid inclusion study

Petrographic observations and fluid inclusion types

At La Crocetta, the mineral assemblage of the first alteration event is absent, suggesting that the corresponding fluids never interacted with rocks outcropping in this area. Therefore, as detailed below, fluid inclusions used in this study are considered to be associated with either the second or the third alteration stages.

Unfortunately, quartz most closely related to the sericitization event, i.e. occurring in the groundmass of eurite samples intimately intergrown with sericite, has a very small crystal size (< 5 μm). Therefore, it is not amenable to microthermometric studies. However, magmatic quartz in eurites almost systematically hosts, along healed fractures, randomly-oriented trails of (secondary) 5 to 20-μm fluid inclusions (Fig. 7a–f). As detailed below, some of these inclusion trails are in physical continuity

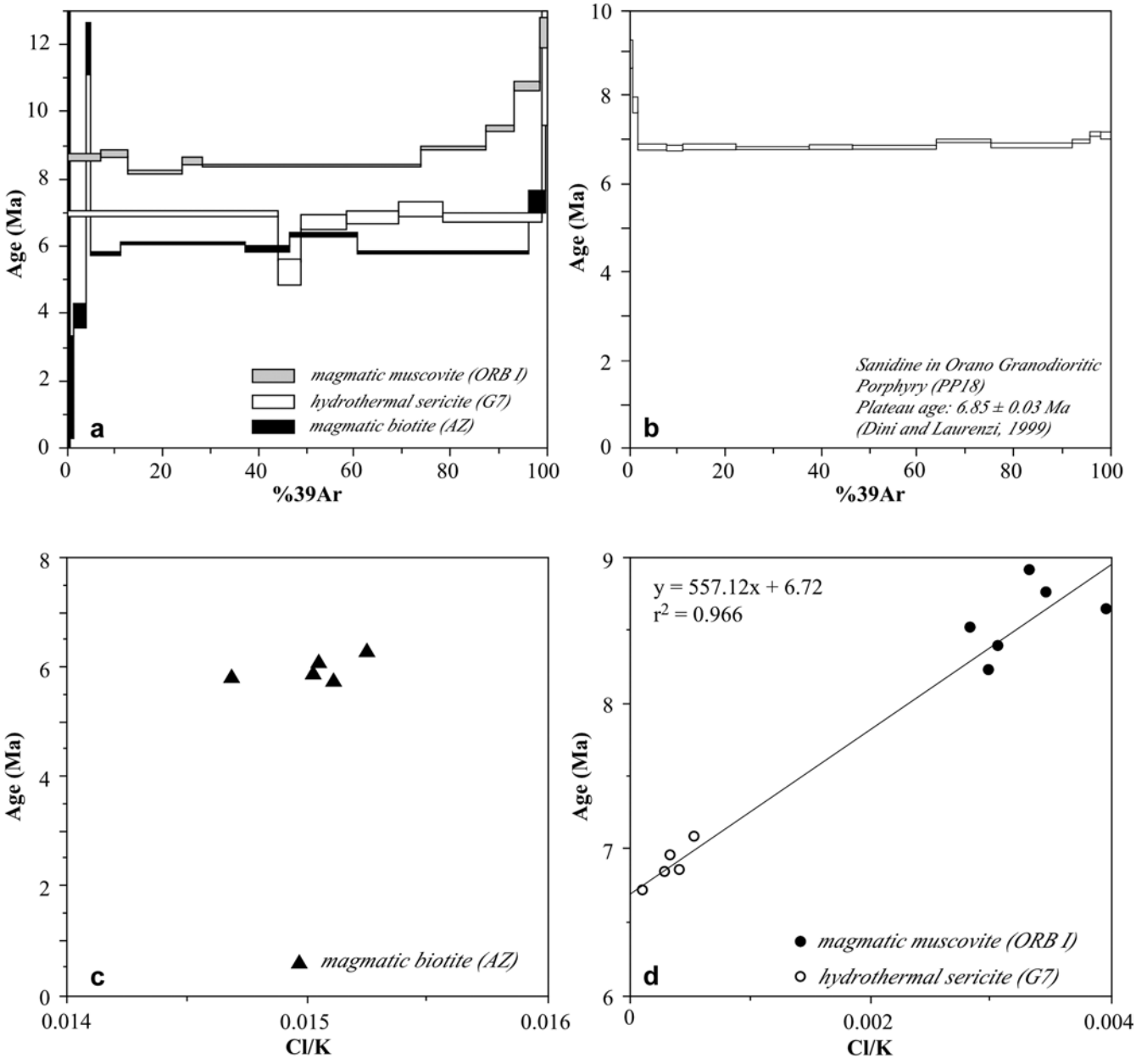

Fig. 6 **a** Released ^{39}Ar vs. age (Ma) spectra for ORB I, G7 and AZ samples; **b** ^{39}Ar vs. age (Ma) spectra for magmatic sanidine in the Orano Granodioritic Porphyry (from Dini and Laurenzi 1999); **c** Cl/K ratio vs. age for AZ biotite; **d** for ORB I muscovite and G7 sericite; the equation of the line obtained by interpolating data points is shown in the *upper left of the box*. See text for details

with calcite + quartz veins of the third alteration stage (Fig. 7b). This textural evidence, along with microthermometric data consistent with those of inclusions trapped in third stage minerals (see below), suggests that these fluids are representative of the third alteration stage. Several other inclusions trails, on the other hand, do not show any obvious relationship to third stage veinlets and, in few cases, we can observe that the healed fractures that host such inclusion trails are cut by third-stage veinlets. Moreover, as detailed below, they show different compositions with respect to third-stage fluids. We suggest that these earlier trails were trapped during the second stage of alteration, because (1) similar fluid inclusions are systematically absent in the unaltered Capo Bianco porphyritic aplites and, outside of La Crocetta area, they can be observed only in rocks were there is moderate sericitization of feldspars, and (2) in a few cases, we could observe sericite associated with fluid inclusion trails (Fig. 7a), and even contained (presumably, accidentally trapped, see Roedder 1984) in fluid inclusions (Fig. 7d). Therefore, although the exact timing of entrapment of the fluid inclusion trails cannot be definitively constrained, the above evidence strongly suggests that entrapment of some inclusion trails was coeval with sericitization.

At room temperature, secondary inclusions in 'early' trails within eurite quartz phenocrysts are either

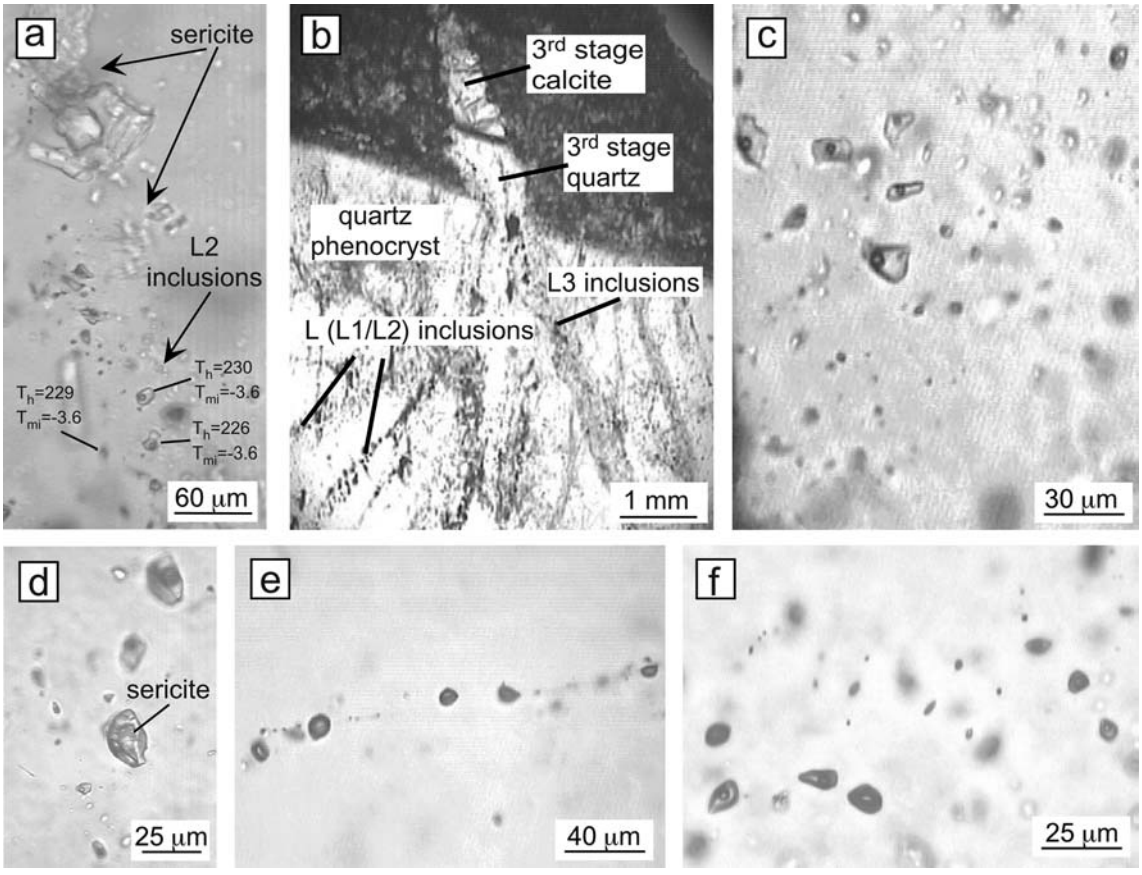

Fig. 7a–f Photomicrographs (transmitted light, parallel nicols) of fluid inclusions hosted in eurite. **a** Fluid inclusion trails (L2) associated with sericite along a healed fracture in magmatic quartz phenocrysts; **b** relict of magmatic quartz phenocrysts crosscut by a third stage microvein, extending outside the crystal, and filled by hydrothermal quartz and calcite. Also shown is a L3 secondary fluid inclusion plane coeval with the third stage microvein, and intragranular L (L1/L2) inclusions within the host quartz. **c** Liquid-rich, two-phase L inclusions in eurite quartz phenocrysts; **d** a L2 inclusion containing sericite (presumably accidentally trapped); **e** vapour-rich, monophase, secondary, V inclusions; **f** coexisting secondary L1 and V inclusions. These inclusions are also shown in the sketch of Fig. 10

liquid-rich (Fig. 7a, c, d) or, more rarely, vapour-rich (Fig. 7e). Most of liquid-rich inclusions are two-phase (aqueous liquid plus vapour), with fairly constant liquid to vapour ratios. By contrast, vapour-rich inclusions have typically variable liquid-to-vapour ratios; they may occur as either two phase (vapour plus minor liquid) or apparently single phase (vapour, although small amounts of liquid, not visible under the optical microscope, may be present). Two groups of liquid-rich inclusions (L1 and L2) were distinguished on the basis of the last solid phase to melt during freezing/heating cycles: clathrate in L1 inclusions, and ice in L2 inclusions (see below). The L1 inclusions are scarce. Most of the L1 and some of the L2 inclusions were observed to occur together, with vapour-rich inclusions, within the same plane (Fig. 7f, see also Fig. 10); in this case, both the liquid- and vapour-rich inclusions can display variable liquid-to-vapour ratios. This evidence may reflect heterogeneous trapping phenomena (i.e. two-phase trapping) and, consequently, this association is interpreted as an indication of coexistence of liquid and vapour (i.e. fluid immiscibility or 'boiling') at trapping conditions (see below).

In both calcite and quartz of the third alteration stage, vapour-rich inclusions are absent and only two-phase, liquid-rich fluid inclusions occur. At least some of these can be considered as primary according to the criteria of Roedder (1984). Inclusions in quartz are usually small in diameter (≤ 5 μm). Only a few inclusions, occurring in third-stage overgrowths on magmatic quartz phenocrysts, could be used for microthemometric observations. On the other hand, where third-stage micro-veins cut the magmatic quartz phenocrysts, many two-phase liquid-rich inclusions suitable for microthermometry are found, aligned along fractures that are apparently continuations of the microveins (Fig. 7b). Microthermometric data from these are similar to those from inclusions in third-stage calcite and in the few primary inclusions studied in the third-stage quartz (see below). To emphasize the different mode of occurrence with respect to the previously described L1 and L2 inclusions, we have labelled all these inclusions that post-date sericitization as L3.

Microthermometric and Raman data

Microthermometric and Raman studies were performed on seven selected samples. The host minerals of the

studied inclusions comprise magmatic quartz phenocrysts in eurite (S2, G11b, G12, G16, CG4), quartz of the third stage (S2), calcite from third-stage macroscopic veins (S5 and S6), and calcite from third-stage calcite–quartz micro-veins (CG4).

Final ice melting (T_{mi}) and homogenization (T_h) temperatures were systematically measured on L1, L2, L3 and V inclusions (Table 3; Figs. 8 and 9). In general, vapour-rich (type V) inclusions, and some L1 or L2 inclusions coexisting with V inclusions, gave inconsistent microthermometric data, with relatively high (generally >250 °C) and widely scattered T_h values. This was interpreted as a consequence of heterogeneous trapping (cf. Table 3). The initial melting temperature (T_e) could be measured only in a few L2 inclusions. During freezing runs, no solid CO_2 was ever observed. Liquid CO_2 was observed only in a few V inclusions. The presence of clathrate on cooling was noted only in L1 inclusions and some V inclusions. However, because of the small size of many L1 inclusions and the poor optical quality of V inclusions, the T_{mcl} could be measured in few inclusions (Table 3), and T_{hCO2} was determined in three V inclusions.

L1 inclusions

The T_{mi} of these inclusions are between –4.8 and –3.8 °C (Table 3, Fig. 8 and 9). The T_{mcl} could be measured in only 11 L1 inclusions, ranging between 3.8 and 5.0 °C. Most L1 inclusions, presumably not heterogeneously trapped and mainly coexisting with V inclusions, show consistent T_h between 212 and 237 °C, with most values between 220 and 230 °C. However, a number of L1 inclusions (all in sample G12) do not reach homogenization for temperatures up to 260 °C. Raman analyses showed that the volatile phase of L1 inclusions is pure CO_2. The computed XCO_2 in these inclusions is 0.025–0.027, whereas the salinity is 3.9–5.2 wt% NaCl equiv.

L2 inclusions

These inclusions are characterized by a rather variable T_{mi} (between –2.5 and –13.2 °C; Table 3, Figs. 8 and 9). Variations may also be large within a single sample. However, the T_{mi} of inclusions belonging to the same plane is, in most cases, relatively constant. The T_{mi} of L2 inclusions coexisting with V inclusions show only small variations, being between about –3.0 and –5.0 °C.

The T_e, measured only in a few large L2 inclusions was between approximately –22 and –30 °C, indicating that, in addition to NaCl, dissolved KCl and/or $MgCl_2$ may be present in the solutions (Crawford 1981). Raman analyses detected the presence of CO_2 in the volatile phase of L2 inclusions. However, no clathrate was observed in these inclusions after final ice melting, probably because clathrate melting occurred at $T \leq T_{mi}$, and could not be recognized in the presence of ice.

Table 3 Summary of fluid inclusion microthermometric results. T_e Initial melting temperature; T_{mi} final ice melting temperature; T_{mcl} clathrate melting temperature; T_h homogenization temperature; *n.o.* not observed. The T_h of fluid inclusions affected by heterogeneous trapping are shown within square brackets. Number of fluid inclusions measured given in parentheses

Sample	T_e (°C)	T_{mi} (°C)	T_{mcl} (°C)	T_h (°C)
L1 inclusions in quartz phenocrysts				
G12	n.o.	–4.8/–4.6 (10)	4.0/5.0 (5)	220/237 (17) [248 (1) >260 (16)]
G11b	n.o.	–3.9 (3)	4.5/4.8 (3)	212/224 (3)
CG4	n.o.	–4.0/–3.8 (2)	3.8/5.0 (3)	223/231 (3)
L2 inclusions in quartz phenocrysts				
G16	–22/–28	–10.6/–3.4 (38)	–	194/226 (38)
G12	–25	–4.1/–2.5 (33)	–	189/230 (31) [249/285 (6)]
G11b	–22/–30	–13.2/–3.2 (23)	–	193/218 (20) [249/261 (3)]
CG4	–22	–10.6/–4.0 (21)	–	183/228 (21)
S2	n.o.	–10.5/–2.9 (35)	–	184/226 (34) [257/264 (3) >270 (4)]
L3 inclusions in quartz phenocrysts				
G12	n.o.	–0.7 (5)	–	180/192 (5)
G11b	n.o.	–1.1/–0.4 (21)	–	193/220 (21)
CG4	n.o.	–0.1 (3)	–	200/210 (3)
L3 inclusions in third stage quartz				
S2	n.o.	–1.2/–0.6 (8)	–	181/213 (8)
L3 inclusions in third stage calcite				
S5	n.o.	–1.5/–1.4 (4)	–	205/211 (4)
S6	n.o.	–1.6/–1.4 (4)	–	197/220 (7)
CG4	n.o.	–0.9/–0.8 (8)	–	211/223 (8)
V inclusions in quartz phenocrysts				
G12	n.o.	n.o.	0.3/10.2 (7)	[235/318 (9) >260 (7)]
G11b	n.o.	n.o.	1.2/2.4 (2)	[270/318 (4) >300 (2)]
CG4	n.o.	n.o.	n.o.	[234/259 (4) >270 (2)]
S2	n.o.	n.o.	7.2 (1)	[>250 (1)]

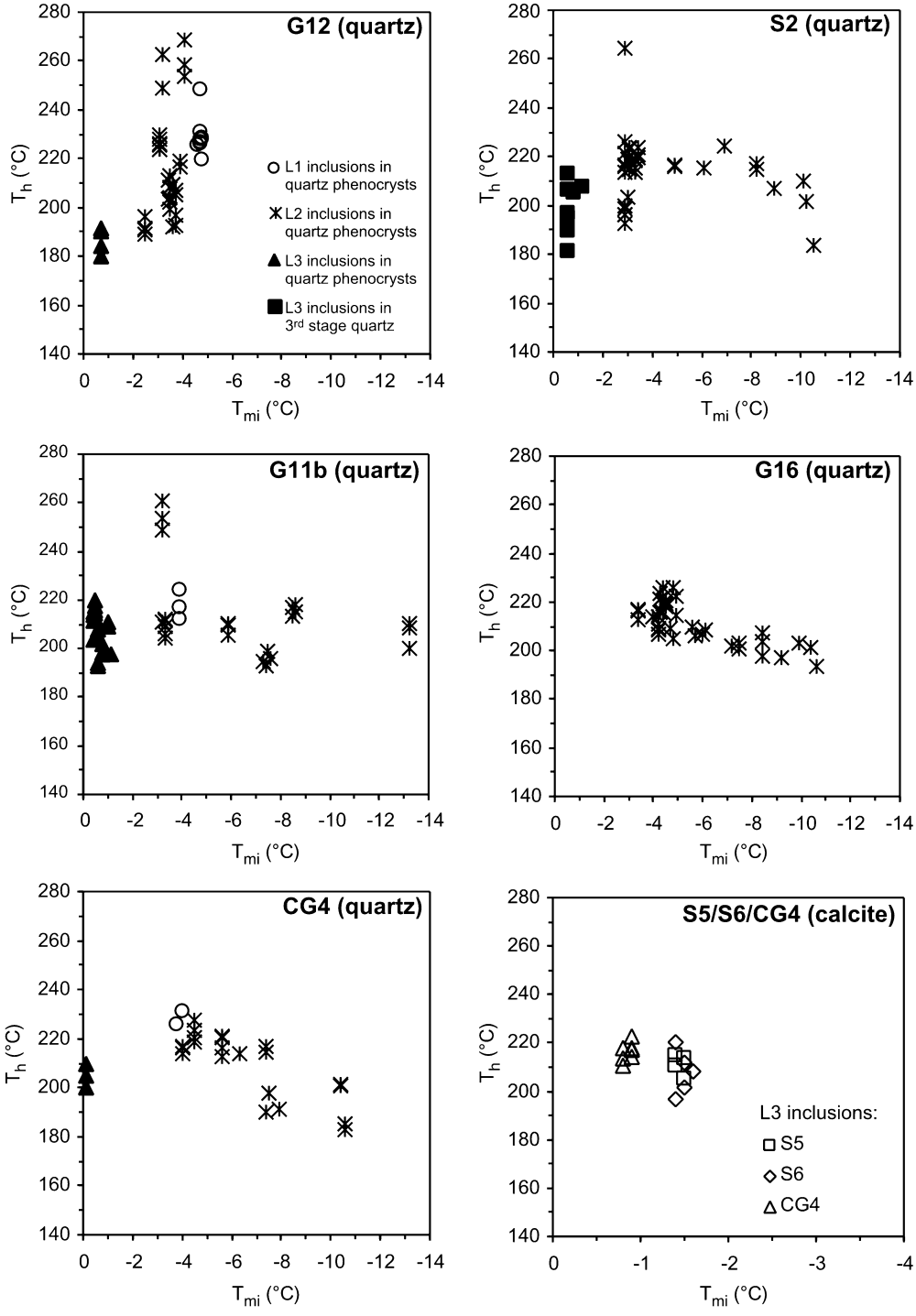

Fig. 8 Plot of homogenization (T_h) vs. final ice melting temperatures (T_{mi}) for fluid inclusions recorded in individual samples

The T_h of L2 inclusions is highly variable (183–285 °C). However, for most of L2 inclusions, which are considered not affected by heterogeneous trapping, the T_h ranged from 183 to 230 °C (Table 3, Figs. 8 and 9), with a mode between 200 and 230 °C. In particular, for L2 inclusions coexisting with V inclusions, T_h ranged from 216 to 230 °C. Again, T_h variations may be significant within a single sample, but different inclusions occurring in the same healed fracture usually show consistent T_h (typically less than 15 °C variation). However, in a few cases, we observed large fluctuations of both T_{mi} (≈7 °C) and T_h (≈25–29 °C) in the same trail.

The CO_2 content of L2 inclusions cannot be precisely estimated. Nevertheless, from the observation that clathrate is not present after T_{mi}, the maximum possible XCO_2 content of L2 inclusions, calculated assuming that $T_{mi} = T_{mcl}$, is 0.014. The salinity of L2 inclusions, calculated from T_{mi}, ranges from 4.2 to 17.1 wt% NaCl equiv., with most values between 4.2 and 7.9 wt% NaCl equiv. Because of the presence of dissolved CO_2 (≤ 0.8 molal),

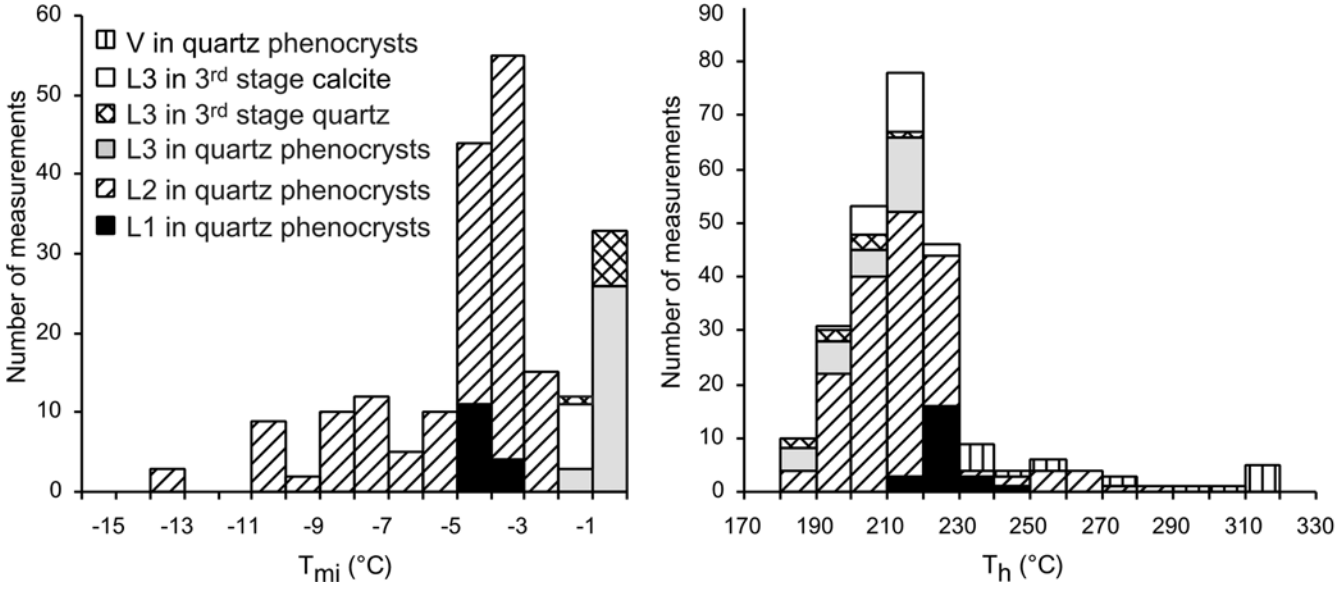

Fig. 9 Frequency histograms for final ice melting (T_{mi}) and homogenization (T_h) temperatures for all inclusions

which depresses the T_{mi} value by as much as 1.4 °C (Hedenquist and Henley 1985), these salinities may have been overestimated by as much as 2.4 wt% NaCl.

L3 inclusions

This type of inclusions in quartz phenocrysts exhibited T_{mi} from –1.1 to –0.1 °C, in third-stage quartz from –1.2 to –0.6 °C, and in calcite from –1.6 to –0.8 °C (Table 3, Figs. 8 and 9). The T_h of L3 inclusions in both magmatic quartz phenocrysts and third-stage quartz was in the range of 180 to 220 °C, with most values falling between 190 and 220 °C. The T_h of L3 in calcite ranged between 197 and 223 °C, with most of the values between 200 and 220 °C (Figs. 8 and 9).

Clathrate was not observed after T_{mi} in L3 inclusions. Hence, their maximum XCO_2 content, computed assuming that $T_{mi} = T_{mcl}$, is 0.015.

The salinity of L3 inclusions in quartz phenocrysts, in third-stage quartz and calcite, estimated from T_{mi}, ranges from 0.2 to 1.9 wt% NaCl equiv., from 1.1 to 2.1 wt% NaCl equiv., and from 1.4 to 2.6 wt% NaCl equiv., respectively. For L3 inclusions, the maximum over-estimation of salinity because of the possible presence of dissolved CO_2 in the fluid is 2.5 wt% NaCl equiv. Microthermometry does not indicate any systematic difference between inclusions hosted by calcite or quartz, nor in veins of different thickness, supporting the concept that they all trapped the same fluid.

V inclusions

Measurements of T_{mcl} and T_h were conducted only in some two-phase V inclusions. Actually, in most V inclusions, clathrate was observed during freezing, but T_{mcl} (between 0.3 and 10.2 °C) could be measured only in ten inclusions. In three inclusions, where the formation of liquid CO_2 occurred on freezing, T_{hCO_2} (to V) was found to range between 10 and 15.3 °C. Raman analyses showed that the volatile phase of these inclusions consists of CO_2. The T_h of V inclusions ranged between 234 and 318 °C. In some quartz fragments, not heated to high temperatures in order to avoid the decrepitation of liquid-rich inclusions, most of the V inclusions did not homogenize during heating to temperatures as high as 250 °C. These T_h data must be regarded with caution, as T_h measurements made on vapour-rich inclusions usually suffer from large errors because of the small quantities of liquid (Roedder 1984; Sterner 1992). In addition, the wide range of T_h of V inclusions suggests that most of the analysed inclusions could have trapped some liquid together with the vapour.

A reliable computation of the bulk compositions of the V inclusions would require an accurate estimation of the volume fraction occupied by the vapour (or liquid) phase, which is >0.90 in many V inclusions. However, the optical characteristics and rather variable liquid-to-vapour ratios of V inclusions do not permit a precise estimate, leading to large uncertainties in the calculated bulk compositions. For example, the bulk compositions of the V inclusion showing T_{hCO_2} of 15.2 °C and T_{mcl} of 9.4 °C, calculated assuming a volume fraction of the gas phase of 0.95, would be $XH_2O = 0.42$ and $XCO_2 = 0.58$ (neglecting the NaCl content of the aqueous phase); if the volume fraction of the gas phase were 0.99, the calculated composition would be $XH_2O = 0.12$ and $XCO_2 = 0.88$. For the same inclusion, the salinity calculated from T_{mcl} is 1.7 wt% NaCl equiv. This is apparently too high for an initially homogeneous vapour phase (at 250 °C the NaCl content of aqueous vapour in equilibrium with a liquid of 5 wt% NaCl is practically

zero), and suggests that, also for this inclusion, trapping was not homogeneous (i.e. a small amount of liquid was trapped along with the vapour).

Evidence of fluid immiscibility and salinity variation

The presence of coexisting L1 and V inclusions, and of L2 and V inclusions, can be produced by (1) the casual trapping of immiscible liquid and vapour phases, or (2) post-trapping processes (including necking-down and leakage upon re-equilibration). The combined inspection of textures and microthermometric data may help to resolve this ambiguity. As an example, in Fig. 10, we show L1 and V inclusions found along a plane (sample G12), and their T_h data. It can be observed that there is little textural evidence of necking-down and/or post-entrapment re-equilibration processes (such as decrepitation features). It is also unlikely that necking down of one or more large liquid-rich inclusions produced the abundant and, in many cases, relatively large V inclusions coexisting with the L1 inclusions. Therefore, fluid immiscibility is the most likely process to form coexisting L1 + V and L2 + V inclusions. The presence of healed fractures in quartz phenocrysts containing only V-type inclusions, indicating that a separate vapour-phase was at times present in the hydrothermal system, further supports this conclusion.

If coexisting L1 + V and L2 + V inclusions were homogeneously trapped, then they should homogenize at the same temperature. However, V inclusions and some of coexisting L1 and L2 inclusions display a rather variable T_h. This is typically interpreted as a consequence of heterogeneous trapping of two immiscible fluids (Roedder 1984; Bodnar et al. 1985). Nevertheless, the lowest T_h of V inclusions, in some cases, falls in the range of T_h of the associated L1 or L2 inclusions, as can be observed for the coexisting L1 + V inclusions in Fig. 10. Thus, the criterion of the same homogenization temperature for coexisting vapour-rich and liquid-rich inclusions trapped during immiscibility (cf. Roedder 1984) is, at least in part, satisfied.

The significant salinity variations displayed by L2 inclusions (~4–17 wt% NaCl equiv.) may be, in part, ascribed to adiabatic boiling processes. However, large salinity increases will only arise from open-system isothermal boiling, where the heat is supplied by the country rocks. In a shallow, liquid-dominated system, such as La Crocetta, isothermal boiling occurs rarely, and could explain only local, isolated high salinity enrichment (cf. Simmons and Browne 1997). The presence of CO_2 (even in small amounts) in the volatile phase of the saline L2 inclusions, demonstrated by the Raman analyses, is also incompatible with a protracted phase separation with vapour (and CO_2) loss. Thus, the higher salinity L2 inclusions are most likely the result of an influx of external saline fluids into the hydrothermal system.

Fig. 10 Sketch of coexisting secondary L1 and V inclusions observed along a healed fracture in a relict magmatic quartz phenocrysts of sample G12. The homogenization temperature (in °C) measured for L1 and V inclusions are reported close to the inclusions. The *inset* shows a photomicrograph of some fluid inclusions of the sketch

P–T–*X* properties of hydrothermal fluids at La Crocetta

Fluid inclusions provide direct information on the physico-chemical nature and on the evolution of the

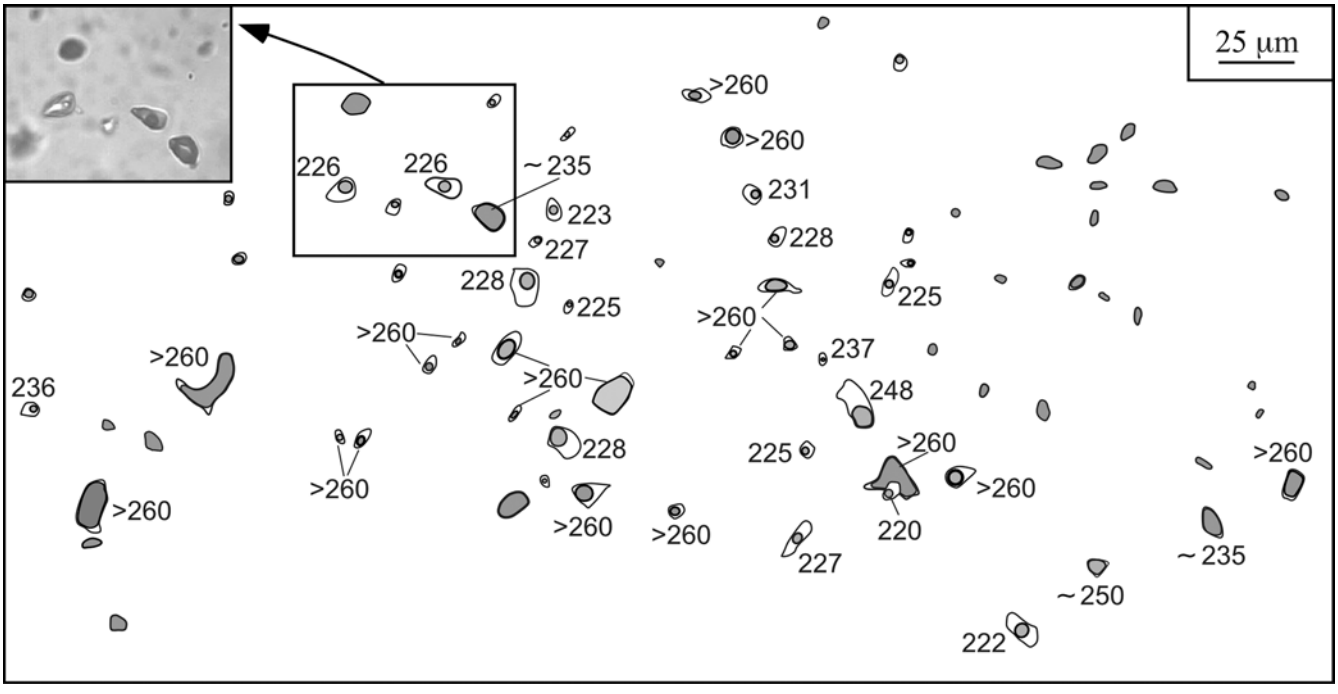

hydrothermal fluids circulating at La Crocetta. In particular, fluids causing the extensive sericitization may be represented by those trapped in L1 and/or L2 inclusions, whereas textural evidence indicates that L3 fluid inclusions were trapped after sericitization.

The trapping sequence of L1 and L2 inclusions is not obvious from textural relationships. However, further indications come from microthermometric studies, and the evidence of boiling and mixing processes. It is possible that the L1 fluid, with its higher CO_2 content ($XCO_2 = 0.025$–0.027), represents a relatively early, gas-rich hydrothermal fluid. It was trapped during an immiscibility process, which produced an episode of CO_2-bearing phase separation (Drummond and Ohmoto 1985). The unmixed, CO_2-depleted liquid could be represented by that trapped in the L2 inclusions, with $XCO_2 \leq 0.014$ and salinity values ≤ 7.9 wt% NaCl equiv. ($T_{mi} < -5$ °C), which is close to the salinity of L1 inclusions.

The trapping conditions of the unmixed L1 and L2 inclusions can be estimated directly from their microthermometric data. The T_h ranges of L1 and L2 inclusions coexisting with V inclusions (212–237 and 216–230 °C, respectively) indicate that these inclusions were trapped at similar temperatures. Trapping pressures of about 280–310 bar were calculated for seven L1 inclusions on the basis of their T_h and composition. By considering the mean salinity of L2 inclusions trapped at boiling, we have calculated the highest possible trapping pressures (about 145 bar) on the basis of the maximum CO_2 content ($XCO_2 = 0.014$) of such inclusions, for the extreme T_h values (216 and 230 °C). The estimated P–T conditions of trapping for L1 and L2 inclusions are in good agreement with the properties of the system H_2O–CO_2–NaCl (curves A, B and C in Fig. 11), as extrapolated from the experimental data of Takenouchi and Kennedy (1965). According to these calculations, there would have been a significant pressure drop (at least of 135 –165 bar) between the trapping of L1 and L2 inclusions. Such a large pressure decrease, without significant temperature variation, can be related to a transition from lithostatic to hydrostatic conditions. If boiling of the CO_2-bearing L1 fluid occurred under lithostatic conditions, then the depth of fluid trapping was around 1,100–1,200 m, considering an average rock density of 2.6 g/cm^3. At this depth, the hydrostatic pressure is approximately 100–110 bar, assuming an average fluid density value (0.94 g/cm^3), which is intermediate between the minimum density of L2 inclusions and the density of cold water. Thus, after the first boiling event recorded by L1 inclusions and partial CO_2 loss, fluid boiling processes continued under hydrostatic pressure (100–110 bar), indicating that the system was open to the surface.

For other L2 inclusions (in particular, for those L2 inclusions that trapped the most saline fluid) and for all L3 inclusions, trapping under boiling conditions cannot be demonstrated because of the absence of associated V inclusions. These inclusions could have formed under either hydrostatic or lithostatic pressure. In both cases, pressure corrections should be added to T_h to obtain the trapping temperatures. However, these corrections are modest (≤ 6 °C, assuming that the depth of inclusion formation did not change, for hydrostatic conditions; < 20 °C for lithostatic conditions). The rather wide range of T_h displayed by L2 inclusions (not affected by heterogeneous trapping) with T_{mi} of about –2.5 to –4.0 °C, and by L3 inclusions, can be related to fluid temperature fluctuations or to trapping at different pressure conditions. In fact, inclusions with lower T_h could be trapped under lithostatic pressure at temperatures similar to those for inclusions that were trapped under hydrostatic pressure.

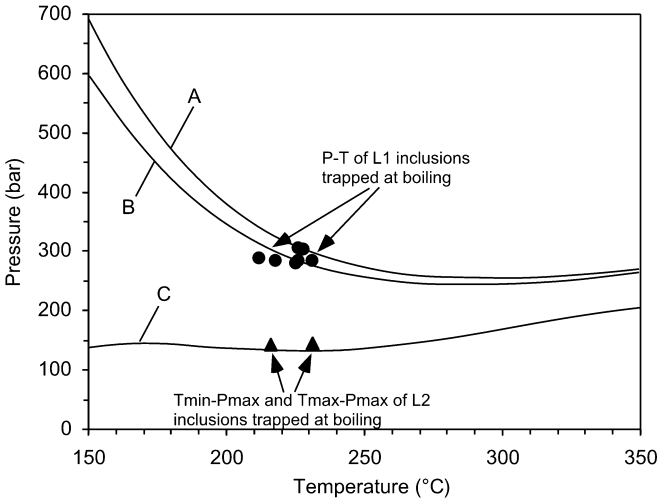

Fig. 11 Pressure (P)–temperature (T) conditions calculated for seven L1 (boiling) inclusions. The trapping pressures for these inclusions were calculated from their microthermometric data and composition, using the method of Barton and Chou (1993). The highest possible trapping pressure (P_{max}) for L2 inclusions, presumably trapping during boiling, with maximum (T_{max}) and minimum (T_{min}) homogenization temperatures, are also shown. *A*, *B*, *C*, are bubble point curves for fluids with *A* 6.3 wt% CO_2 (XCO_2 ~0.027), *B* 6.0 wt% CO_2 (XCO_2 ~0.025) and *C* 3.4 wt% CO_2 (XCO_2 ~0.014), all with a salinity of 6.0 wt% NaCl (relative to the H_2O–NaCl subsystem), calculated from Takenouchi and Kennedy's (1965) experimental data (see text for details)

Discussion

Potassium metasomatism at La Crocetta

Petrographic evidence and mass balance calculations show that, at the La Crocetta mine, the exploited potassium-rich rocks are the result of potassium metasomatism and pervasive sericitization of primary feldspars. Such a process is widely documented in a variety of ore deposits (e.g. porphyry systems, epithermal base and precious metal deposits), where secondary K-feldspar and/or K-mica form depending on pH and bulk chemistry (Lowell and Guilbert 1970; Hayba et al. 1985; Henley 1985). The peculiar feature of La Crocetta is that

sericite, usually a minor and uneconomic phase is, in fact, the true ore mineral. Moreover, in contrast to what normally happens in deposits affected by intense K^+ metasomatism (cf. Meyer and Hemley 1967), at La Crocetta the sericitic alteration represented the main step of K^+ enrichment in the system.

The process of sericitization by replacement of both albite and K-feldspar can be schematized as follows:

$$12\ \text{Albite} + 3\ \text{K} - \text{feldspar} + 2\ K^+ + 10H^+ = 5\ \text{K} - \text{mica} + 30\ SiO_2 + 12\ Na^+ \quad (1)$$

In agreement with mass balance calculations, the reaction requires the introduction of potassium, and the removal of sodium from the system. Mass balance calculations (supported by petrographic evidence) also suggest that most of the released silica remained in the system as newly formed microcrystalline quartz.

Hydrothermal fluids

Large-scale feldspar hydrolysis of the protolith might have developed in the presence of a CO_2-bearing L1 fluid and/or of a partially degassed L2 solution. The presence of CO_2 in the L1 inclusions ($XCO_2 = 0.027$–0.022) and, in lesser amounts, in the L2 inclusions ($XCO_2 \leq 0.014$) suggests slightly acidic fluids, in agreement with the hypothesis that they were in equilibrium with sericite. This CO_2 could have been lost during boiling episodes, thereby raising the pH of the residual liquid (cf. Drummond and Ohmoto 1985). However, all the L2 inclusions analysed by Raman spectroscopy contain some CO_2, suggesting that either fluid boiling (with attendant CO_2 loss) occurred only as transient episodes, consuming only in part the CO_2 dissolved in the fluid; or CO_2 was continuously supplied from an external (magmatic?) source. In any event, pH variations were constantly confined within the stability field of sericite.

Pressure during sericitization probably oscillated between lithostatic (280–310 bar) and hydrostatic (100–110 bar) values, and temperatures were mostly in the 190–240 °C range. In general, the salinities of L1 and L2 fluids were moderate (3.9–7.9 wt% NaCl equiv.); however, some L2 inclusions also record the injection into the hydrothermal system of higher salinity fluids (up to 17 wt% NaCl equiv.).

Information on the source(s) of metasomatizing fluids can be tentatively derived from fluid inclusion characteristics. The moderate salinity and formation temperatures of L1 and of most L2 inclusions do not suggest a dominantly magmatic fluid, and are more typical of fluids of meteoric nature. On the other hand, the source(s) of the fluids with higher salinity recorded by some L2 inclusions remains problematic. It cannot be explained by an involvement of evaporitic sediments because these are not known in central-western Elba Island. Given the geological context, a magmatic contribution is certainly possible, but not demonstrated.

Further insights into ore fluid source(s) at La Crocetta can be provided by the relatively high K/Rb ratio of altered rocks (eurites). Residual "granitic" hydrothermal fluids usually show a lower K/Rb ratio (Beswick 1973). Typical magmatic ore fluids, such as those present in porphyry Cu–Au, Sn–W greisen, pegmatites and in some epithermal systems, are rubidium-rich, and produce alteration haloes with low K/Rb ratio (as low as 50; Kerrich and Fryer 1988; Kerrich 1989), where the two elements are consistently co-enriched (Silberman and Berger 1985; Kerrich 1989, and references therein).

Hence, although the ultimate fluid source of the second alteration event at La Crocetta remains poorly constrained, it is unlikely that fluids responsible for sericitization were derived from local 'granitic' fluid sources, such as monzogranitic porphyries and the two monzogranitic plutons. Moreover, any involvement of the Porto Azzurro pluton in the sericitization process conflicts with both field evidence (the extent of sericitization increases eastwards, i.e. away from the pluton and toward the Elba Centrale fault surface) and the ^{40}Ar–^{39}Ar age of sericitization (6.7 Ma), which is distinctly older than the cooling age of the pluton (ca. 5.9 Ma). The only magmatic rocks of Elba Island that have a comparatively high K/Rb ratio (~150) are the more mafic OGP. As previously reported, they have about the same ^{40}Ar–^{39}Ar age as the sericitization, and reconstruction of pre-detachment geometry shows that at about 7 Ma an exchange of fluids between OGP and Capo Bianco aplites at La Crocetta would be possible (Fig. 12).

The late-stage carbonate (± pyrite ± quartz) veins and the 'candor' facies are associated with the circulation of L3 fluids. The latter are characterized by a relatively low salinity, whereas T_h are still comparable with L1 and L2 fluids. Conceivably, L3 fluids record the late ingression of a meteoric water into the hydrothermal system at the La Crocetta mine. This conclusion is also suggested by preliminary oxygen isotopic data on calcite (Maineri et al. 1998).

Fluid circulation model

In summary, we suggest that eurites were formed by sericitic alteration of Capo Bianco porphyritic aplite in a syn-kinematic extensional regime, which allowed the migration of hydrothermal fluids mostly along low-angle tectonic lineaments of regional importance (Elba Centrale fault). There are a number of similarities with the potassium metasomatism accompanying Tertiary crustal extension in the south-western United States, where several base- and precious-metal deposits are located along detachment faults (e.g. Davis et al. 1986; Roddy et al. 1988). By contrast, at the regional scale, the La Crocetta deposit differs significantly by its mineralization style and structural controls from other late- to post-orogenic Cu–Pb (Ag)–Zn and Hg–Sb ore deposits of southern Tuscany. Many of these deposits, in fact, are

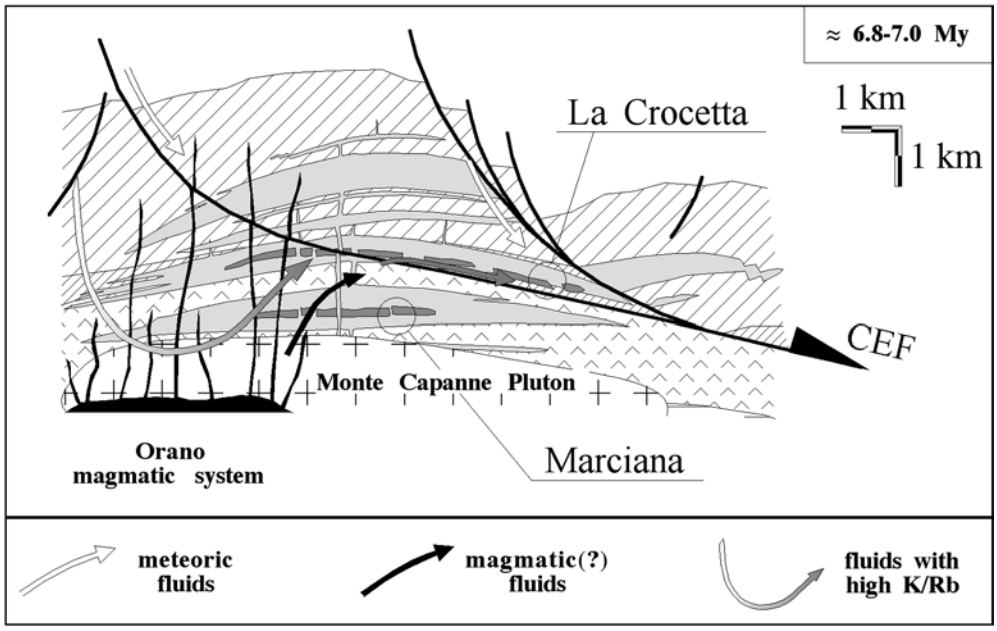

Fig. 12 Cartoon illustrating the inferred relationships among Capo Bianco porphyritic aplite, OGP and mineralizing fluids, flowing along the Elba Centrale fault. The relative positions of Marciana and La Crocetta Capo Bianco porphyritic aplite bodies are also shown. *Symbols* as in the legend of Fig. 2

clearly linked to the late high-angle extensional tectonics (cf. Lattanzi et al. 1994) affecting the northern Tyrrhenian area when the low-angle extensional faults (like Elba Centrale fault at Elba) had completely ceased their activity.

The volumetric properties of L1 boiling fluids suggest that sericitization took place at a depth of about 1,100–1,200 m. Westerman et al. (2000), based on reconstructed geological cross sections in western and central Elba, suggested a depth of about 3,000 m for the Elba Centrale fault plane. However, their estimate does not take into account the crustal thinning, accomplished by Miocene–Pliocene extensional tectonism, as evidenced by fieldwork, boreholes and geophysical studies in southern Tuscany (e.g. Carmignani et al. 1994) and in the northern Tyrrhenian Sea (e.g. Bartole 1995). Our data would, therefore, indicate that the locus of ore deposition was in close proximity to the fault plane. The negligible sericitization in the western outcrops of Capo Bianco porphyritic aplite (Marciana area) may be ascribed mainly to the their location within the footwall zone of the Elba Centrale fault, which precluded their interaction with the syn-kinematic hydrothermal system (Fig. 12).

Conclusions

At the La Crocetta mine, high quality raw ceramic material (eurite) was produced by pervasive sericitic metasomatism of a >8.5-Ma alkali-feldspar granitic (Capo Bianco porphyritic aplite) protolith. This process modified mineralogy and chemistry of Capo Bianco porphyritic aplite, changing the original alkali ratios of the rock ($K_2O/Na_2O \cong 1$) toward a potassium-rich, sodium-poor composition (K_2O/Na_2O up to $\cong 60$).

Fluid inclusion studies suggest that potassium-metasomatism can be related to the circulation of fluids with temperatures mostly between 190 and 240 °C, characterized by both variable salinity (4–17 wt% NaCl equiv.) and CO_2 content ($XCO_2 = 0.025$–0.027 or $XCO_2 \leq 0.014$). Late stage carbonate (± quartz ± sulfide) veining, which detracts from the commercial quality of the rock, involved fluids of meteoric origin.

Mass balance calculations indicate that sericitization was accompanied by potassium gain and sodium (± Ca–Fe) loss, whereas rubidium was essentially immobile. Hence, it appears that the K/Rb ratio of the ore fluids was definitely different from that expected for any residual magmatic fluid from Capo Bianco porphyritic aplite. Moreover, Ar–Ar age estimates suggest that the emplacement of Capo Bianco aplite pre-dates sericitization by about 2 million years. On this basis, we conclude that sericitization is not the result of emplacement of the Capo Bianco porphyritic aplite. Field evidence, K/Rb geochemistry and age estimates also suggest that the Porto Azzurro pluton (5.9 Ma) was not involved in the sericitization process.

Field evidence emphasizes the role of the Elba Centrale fault as the main channel for the ore-forming fluids. Reconstruction of the pre-detachment geometry, and the ^{40}Ar–^{39}Ar estimated age of sericitization (about 6.7 Ma), give permissive evidence of a possible link between the high K/Rb Orano granodiorite porphyries (6.85 Ma) and sericitization. However, the exact nature of this link (if any) remains at this stage speculative.

The main implication for exploration from the newly proposed model is that any orebody similar to La Crocetta should be preferentially sought in the upper plate (hanging wall) of the Elba Centrale fault detachment system. It is unlikely that the portions of Capo Bianco porphyritic aplite bodies localized in the lower plate

(footwall) of Elba Centrale fault were affected by potassium metasomatism, as a consequence of either their deep emplacement and/or the comparatively limited infiltration of meteoric fluids into rocks of the lower plate.

Acknowledgements This study was initiated at the suggestion and under the supervision of Professor Giuseppe Tanelli. Some field and chemical data reported here were collected during undergraduate thesis work at Università di Firenze by M. Luccarini and L. Peruzzi. Mr A. Bertoni and the whole EURIT mine staff are thanked for their kind assistance during fieldwork and sample collection. G. De Grandis of IGGI-CNR in Pisa is thanked for her precious help during mineral separation. Finally, we appreciate the constructive criticism on the first submitted version of the manuscript by Anthony Fallick and an anonymous reviewer, and the painstaking editorial effort by Richard Goldfarb.

References

Bakker RJ (1997) Clathrates: computer programs to calculate fluid inclusion V-X properties using clathrate melting temperatures. Comput Geosci 23:1–18

Barberi F, Dallan L, Franzini M, Giglia G, Innocenti F, Marinelli G, Raggi R, Ricci CA, Squarci P, Taffi L, Trevisan L (1967) Carta geologica dell'Isola d'Elba alla scala 1:25,000. Servizio Geologico d'Italia, Roma

Barberi F, Brandi GP, Giglia G, Innocenti F, Marinelli G, Raggi G, Ricci CA, Squarci P, Taffi L, Trevisan L (1969a) Carta Geologica d'Italia, Scala 1:100,000. Foglio 126 (Isola d'Elba) Servizio Geologico d'Italia, Ed. Servizio Geologico d'Italia, Roma

Barberi F, Dallan L, Franzini M, Giglia G, Innocenti F, Marinelli G, Raggi R, Squarci P, Taffi L, Trevisan L (1969b) Note Illustrative Carta Geol d' Italia. Foglio 126 (Isola d'Elba) Servizio Geologico d'Italia

Bartole R (1995) The North Tyrrhenian–northern Apennines post-collisional system: constraints for a geodynamic model. Terra Nova 7:7–30

Barton PB, Chou IM (1993) Refinement of the evaluation of the role of CO_2 in modifying estimates of pressure of epithermal mineralization. Econ Geol 88:873–884

Beswick AE (1973) An experimental study of alkali metal distribution in feldspars and mica. Geochim Cosmochim Acta 37:183–200

Bodnar RJ, Vityk MO (1994) Interpretation of microthermometric data for H_2O–NaCl fluid inclusion. In: De Vivo B, Frezzotti ML (eds) IMA '94: short course on fluid inclusions, Pontignano–Siena. 1–4 September 1994,Virginia Polytechnic Institute and State University, Virginia, pp 117–130

Bodnar RJ, Reynolds TJ, Kuehn CA (1985) Fluid-inclusion systematic in epithermal systems. Rev Econ Geol 2:73–97

Bortolotti V, Babbini A, Corti S, Dini C, Fazzuoli M, Pandeli E, Principi G (2001) The geology of the central-eastern Elba. Ofioliti 26(2a):97–150

Bouillin JP, Popeau G, Sabil N (1994) Etude thermo-chronologique de la dénudation du pluton du Monte Capanne (Ile d'Elbe, Italie) par les traces de fission. Bull Soc Geol Fr 165:19–25

Carmignani L, Decandia FA, Fantozzi PL, Lazzarotto A, Liotta D, Meccheri M (1994) Tertiary extensional tectonics in Tuscany (northern Apennines, Italy). Tectonophysics 238(1–4):295–315

Crawford ML (1981) Phase equilibria in aqueous fluid inclusion. In: Hollister LS, Crawford ML (eds) Short course in fluid inclusion. Mineral Assoc Can 6:75–100

Daniel JM, Jolivet L (1995) Detachment faults and pluton emplacement: Elba Island (Tyrrhenian Sea). Bull Soc Geol Fr 166:341–354

Davis GA, Lister GS, Reynolds SJ (1986) Structural evolution of the Whipple and South Mountains shear zones, southwestern United States. Geology 14:7–10

Dini A (1997) Le rocce porfiriche dell'Isola d'Elba: geologia, geocronologia e geochimica. PhD Thesis, Università di Pisa, Italy. English abstr in Plinius 17:130–136

Dini A, Laurenzi MA (1999) $^{40}Ar/^{39}Ar$ chronology of shallow-level granitic intrusions, Elba Island, Italy. In: Geoitalia, second Forum FIST 1999, Bellaria 20–23 September 1999, Abstr vol, pp 288–290

Dini A, Tonarini S (1997) Evoluzione tettono-magmatica dell'Isola d'Elba centro-occidentale: nuovi dati geologici e geocronologici sulle Rocce Porfiriche. Convegno Nazionale Progetto CROP (Crosta Profonda), Trieste 23–24 Giugno 1997 (unpaginated abstract)

Dini A, Innocenti F, Rocchi S, Tonarini S, Westerman DS (2002) The magmatic evolution of the laccolith–pluton–dyke complex of Elba island, Italy. Geol Mag (in press)

Drummond SE, Ohmoto H (1985) Chemical evolution and mineral deposition in boiling hydrothermal system. Econ Geol 80:126–147

Ferrara G, Tonarini S (1985) Radiometric geochronology in Tuscany: results and problems. Rendiconti Soc Ital Mineral Petrol 40:111–124

Grant JS (1986) The isochon diagram – a simple solution to Gresen's equation for metasomatic alteration. Econ Geol 81:1976–1982

Hayba DO, Bethke PM, Heald P, Foley NK (1985) Geologic, mineralogic and geochemical characteristics of volcanic-hosted epithermal precious-metal deposits. In: Berger BR, Bethke PM (eds) Geology and geochemistry of epithermal systems. Rev Econ Geol 2:129–168

Hedenquist JW, Henley RW (1985) The importance of CO_2 on freezing point measurements of fluid inclusions: evidence from active geothermal systems and implications for epithermal ore deposition. Econ Geol 80:1379–1406

Henley RW (1985) The geothermal framework for epithermal deposit. In: Berger BR, Bethke PM (eds) Geology and geochemistry of epithermal systems. Rev Econ Geol 2:1–24

Innocenti F, Serri G, Ferrara G, Manetti P, Tonarini S (1992) Genesis and classification of the rocks of Tuscan magmatic province: thirty years after Marinelli's model. Acta Vulcanol Marinelli Vol 2:247–265

Juteau M, Michard A, Zimmermann JL, Albarede F (1984) Isotopic heterogeneities in the granitic intrusion of Monte Capanne (Elba Island, Italy) and dating concepts. J Petrol 25:532–545

Keller JV, Pialli G (1990) Tectonics of the Island of Elba: a reappraisal. Boll Soc Geol It 109:413–425

Kerrich R (1989) Geochemical evidence on the source of fluids and solutes for shear zone-hosted mesothermal gold deposits. In: Bursnall JT (ed) Mineralization and shear zones. Geol Assoc Can Short Course Notes 6:89–128

Kerrich R, Fryer BJ (1988) Lithophile-element systematics of Archean greenstone belt Au–Ag deposits: implication for source process. Can J Earth Sci 25:945–953

Lattanzi P, Benvenuti M, Costagliola P, Tanelli G (1994) An overview of recent research on the metallogeny of Tuscany, with special reference to the Apuane Alps. Mem Soc Geol Ital 48:613–625

Lowell JD, Guilbert JM (1970) Lateral and vertical alteration-mineralization zoning in porphyry copper deposits. Econ Geol 65:373–408

Ludwig KR (2001) Isoplot/Ex, version 2.49: a geochronological toolkit for Microsoft Excel. Berkeley Geochronology Center, Special Publication no 1

Maineri C, Costagliola P, Benvenuti M, Ruggieri G, Casiglia A, Vaselli O, Lattanzi P, Tanelli G (1998) Studies of the 'La Crocetta' raw ceramic material mine (Porto Azzurro, Isola d'Elba): fluid inclusion and C–O isotope constraints of late stage fluids. Plinius 20:143–144

Marinelli G (1955) Le rocce porfiriche dell' Isola d' Elba. Atti Soc Tosc Sci Nat Mem, Ser A 62(2):269–417

Marinelli G (1959) Le intrusioni terziarie dell' Isola d' Elba. Atti Soc Tosc Sci Nat Mem, Ser A 66:50–223

Meyer C, Hemley JJ (1967) Wall rock alteration. In Barnes HL (ed) Geochemistry of hydrothermal ore deposits. Holt, Rinehart and Winston, New York, pp 166–235

Pearson K (1998) Italy's minerals. Poised for ceramic markets. Indust Minerals 374:21–39

Pertusati PC, Raggi G, Ricci CA, Duranti S, Palmeri R (1993) Evoluzione post-collisionale dell' Elba centro-orientale. Mem Soc Geol Ital 49:223–312

Roddy MS, Reynolds SJ, Smith BM, Ruiz J (1988) K-metasomatism and detachment-related mineralization, Harcuvar Mountains, Arizona. Geol Soc Am Bull 100:1627–1639

Roedder E (1984) Fluid inclusions. Mineral Soc Am Rev Mineral vol 12, 640 pp

Saupè F, Marignac C, Moine B, Sonet J, Zimmermann JL (1982) Datation par les methodes K/Ar et Rb/Sr de quelques roches de la partie orientale de l' Ile d' Elbe (Province de Livourne, Italie). Bull Mineral 105:236–245

Serri G, Innocenti F, Manetti P, Tonarini S, Ferrara G (1991) Il Magmatismo Neogenico–Quaternario dell'area Tosco-Laziale-Umbra: implicazioni sui modelli di evoluzione geodinamica dell'Appennino Settentrionale. Stud Geol Camerti Spec Issue 1:429–463

Silberman ML, Berger BR (1985) Relationship of trace-elements patterns to alteration and morphology in epithermal precious-metal deposits. Rev Econ Geol 2:203–232

Simmons SF, Browne PRL (1997) Saline fluid inclusions in sphalerite from the Broadlands Ohaaki geothermal system: a coincidental trapping of fluids being boiled toward dryness. Econ Geol 92:485–489

Sterner SM (1992) Homogenization of fluid inclusions to the vapour phase: the apparent homogenization phenomenon. Econ Geol 87:1616–1623

Takenouchi S, Kennedy GC (1965) The solubility of carbon dioxide in NaCl solution at high temperatures and pressures. Am J Sci 263:445–454

Trevisan L (1950) L'Elba orientale e la sua tettonica di scivolamento per gravità. Mem Ist Geol Univ Padova 16:1–36

Villa IM (2001) Radiogenic isotopes in fluid inclusions. Lithos 55:115–124

Villa IM, Ruggieri G, Puxeddu M (1997) Petrological and geochronological discrimination of two white-mica generations in a granite cored from the Larderello-Travale geothermal field (Italy). Eur J Mineral 9:563–568

Villa IM, Hermann J, Müntener O, Trommsdorff V (2000) ^{40}Ar–^{39}Ar dating of multiply zoned amphibole generations (Malenco, Italian Alps). Contrib Mineral Petrol 140:363–381

Villa IM, Ruggieri G, Puxeddu M (2001) Geochronology of magmatic and hydrothermal micas from the Larderello geothermal field. In: Cidu R (ed) Proceedings WRI-10. Balkema, Rotterdam, pp 1589–1592

Westerman DS, Dini A, Innocenti F, Rocchi S, Tonarini S (2000) Christmas-trees in the shallow crust: the nested laccolith complex from Elba Island, Italy (Abstr). Geoscience 2000, Manchester

Zhang YG, Frantz JD (1987) Determination of the homogenization temperatures and densities of supercritical fluids in the system NaCl–KCl–$CaCl_2$–H_2O using synthetic fluid inclusions. Chem Geol 64:335–350

Zitellini N, Trincardi F, Marani M, Fabbri A (1986) Neogene tectonics of the northern Tyrrhenian Sea. Giornale Geol 48:25–40